Vpr drives massive cellular proteome remodelling in HIV-1 infection

Edward JD Greenwood[1*], James C Williamson[1*], Agata Sienkiewicz[1], Adi Naamati[1], Nicholas J Matheson[1], Paul J Lehner[1].

* These authors contributed equally to this work

1. Department of Medicine, CIMR, University of Cambridge, CB2 0XY, UK.

Abstract

Viral infection causes global remodelling of the cellular proteome. We previously mapped the temporal changes in abundance of thousands of proteins in HIV-1 infected cells (Greenwood & Matheson, 2016). While a small proportion of these changes were attributable to specific HIV-1 accessory proteins, most were unexplained. Here, we use complementary unbiased mass spectrometry-based approaches to demonstrate that a single viral protein, Vpr, is both necessary and sufficient to cause the vast majority of these changes. This global protein regulation requires substrate binding and degradation via DCAF1, but is mostly independent of Vpr-mediated cell cycle arrest. Combined approaches of pulsed-Stable Isotope Labelling with Amino Acids in Cell Culture (pulsed-SILAC) and immunoprecipitation-mass spectrometry (IP-MS) identified at least 38 such cellular proteins directly targeted for degradation by Vpr. Thus, whilst other HIV-1 accessory proteins downregulate a small number of host factors, Vpr degrades multiple protein targets, causing systems-level remodelling of the cellular proteome.

Impact statement

HIV infection causes massive changes to the cellular proteome and a single HIV protein, Vpr, is necessary and sufficient to drive almost all these changes by degrading multiple host proteins.

Introduction

The HIV-1 'accessory proteins' Vif, Vpr, Nef and Vpu deplete host proteins in infected cells, and are required for viral replication *in vivo* [1-3]. We previously used unbiased quantitative proteomics to map temporal changes in cellular protein abundance during HIV infection of CEM-T4 T-cells, and identify novel targets of Vpu (SNAT1), Nef (SERINC3/5) and Vif (PPP2R5A-E) [4, 5]. Nonetheless, known accessory protein targets only account for a tiny fraction of all protein changes observed during HIV infection [5]. Since a single accessory protein, Vif, is sufficient to drive global remodelling of the cellular phosphoproteome [5], we hypothesised that undiscovered targets of the accessory protein, Vpr, might explain a proportion of the remaining protein-level changes.

Results

Vpr is required for global proteome remodelling in HIV infected cells.

We compared total proteomes of uninfected cells with cells infected with either WT HIV or an HIV Vpr deletion mutant (HIV ΔVpr) at an infectious MOI of 1.5 (**Figure 1A**), resulting in approximately 75% infection (**Figure 1B**). Data from this experiment are available, together with the other proteomics datasets presented here, in a readily searchable interactive format in **Figure 1—source data 1**. Amongst the 7,774 quantitated proteins, we observed widespread changes in cells infected with wild-type HIV (**Figure 1C** left panel). Together with known Nef, Vpu and Vif, targets, we saw

39 depletion of previously reported Vpr targets including HLTF [6, 7], ZGPAT [8], MCM10 [9], UNG [10],
40 TET2 [11], MUS81 and EME1 [12, 13]. DCAF1, part of the ligase complex used by Vpr to degrade
41 targets was also depleted, consistent with a previous report [14].

42 In HIV ΔVpr infection (**Figure 1C**, right panel), depletion of Nef, Vpu and Vif targets was maintained.
43 Remarkably, as well as abolishing depletion of known Vpr targets, almost all of the previously
44 uncharacterised protein changes were also reduced or abolished in HIV ΔVpr infection. Whilst 1,944
45 proteins changed significantly (q<0.01) in WT HIV-infected cells, only 41 protein changes (2%)
46 retained significance when cells were infected with HIV ΔVpr. Indeed, principle component analysis
47 showed that cells infected with HIV ΔVpr virus share more similarity on the proteome level with
48 uninfected cell than with cells infected with WT virus (**Figure 1D**).

49 **Incoming Vpr protein alone drives massive cellular proteome remodelling.**
50 Since Vpr enhances expression of other viral proteins [15, 16] (**Figure 1C**), differences between WT
51 and ΔVpr viruses could potentially be explained by secondary changes in expression levels of other
52 proteins, or different rates of progression of WT and ΔVpr viral infections. To eliminate these
53 potential confounders, we therefore examined the effect of Vpr alone. Further, unlike other HIV-1
54 accessory proteins, Vpr is specifically packaged into nascent viral particles, and as such, we wanted
55 to examine the effect of this delivered protein. We therefore repeated our proteomic analysis using
56 cells exposed to lentiviral particles lacking or bearing Vpr in the presence of reverse transcriptase
57 inhibitors (RTi). We therefore excluded all *de novo* viral protein expression and examined the
58 changes induced by Vpr-containing viral particles delivered directly from the virion (**Figure 2A**). Cells
59 were exposed to these viral particles at an infectious MOI of 0.5 (determined in the absence of RTi).

60 Strikingly, changes induced by Vpr-containing viral particles phenocopied the Vpr-dependent
61 proteome remodelling seen in HIV infection (**Figure 2B**), with a high degree of correlation (r^2 = 0.67;
62 **Figure 2C**). Taking both experiments together, Vpr is both necessary and sufficient to cause the
63 significant (q<0.01) depletion of at least 302 proteins, and the upregulation of 413 – highlighted in
64 blue and red, respectively (**Figure 2c**). This is a stringent false discovery rate and, in practice, the
65 number of Vpr-dependent changes is almost certainly even higher. Where antibodies were available,
66 we confirmed a proportion of these changes by immunoblot (**Figure 2 – figure supplement 1**).

67 **Cellular proteome remodelling requires interaction with DCAF1 and cellular substrates.**
68 While the function or functions of Vpr remain controversial, in all phenotypic descriptions, Vpr
69 activity is dependent on the interaction between Vpr and the DCAF1/DDB/Cul4 ligase complex,
70 recruitment of which results in ubiquitination and degradation of known Vpr targets through the
71 ubiquitin-proteasome system. Therefore, in addition to testing the effect of wild type Vpr protein
72 delivered in viral particles to the cellular proteome, we tested a number of previously described
73 mutant Vpr variants (See schematic in **Figure 2A** and results in **Figures 2D,E** and additional
74 information in **Figure 2 - figure supplement2**)

75 Since the Q65 residue of Vpr is required for the interaction with DCAF1 [17], we compared proteome
76 changes caused by a Q65R Vpr mutant with WT Vpr. As predicted, the Q65R Vpr was almost
77 completely inactive (**Figure 2D,E**). We recapitulated this finding by comparing the effects of WT Vpr
78 in control cells, or cells depleted of DCAF1 (**Figure 2 – figure supplement 3**). ShRNA mediated
79 depletion of DCAF1 resulted in an approximately 50% reduction in protein abundance of DCAF1

(**Figure 2 – figure supplement 3B**). Depletion of DCAF1 alone did not phenocopy the Vpr mediated proteome remodelling, and the widespread effects of Vpr are therefore unlikely to be only dependent on the Vpr mediated sequestration and/or depletion of DCAF1. As a proportion of cellular DCAF1 was still expressed, known Vpr effects including degradation of HLTF and upregulation of CCNB1 was partially rather than completely inhibited (**Figure 2 – figure supplement C)**. Consistent with this, Vpr mediated changes were broadly reduced in magnitude in the DCAF1 knockdown cells (**Figure 2 – figure supplement 3D)**. Thus, as with depletion of known Vpr targets, extensive Vpr-dependent proteomic remodelling is dependent on Vpr's interaction with its cognate DCAF1/DDB/Cul4 ligase.

Residues E24, R36, Y47, D52 and W54 of Vpr are also required for the recruitment and degradation of previously described Vpr targets, and are reported to form the substrate-binding surface [7, 18, 19]. Y47, D52 & W54 make up the proposed DNA mimicking motif by which Vpr binds the cellular target UNG2 [18]. In agreement, the $Vpr_{E24R, R36P}$ and Vpr_{W54R} mutants showed attenuated remodelling of the proteome, while a triple mutant, $Vpr_{Y47A, D52A, W54R}$, was defective for almost all Vpr-dependent protein changes (**Figure 2D,E**). Global protein remodelling therefore depends on both the substrate binding surfaces of Vpr, and the recruitment of DCAF1, suggesting that this process is mediated by recruiting Vpr substrates to the DCAF1/DDB1/CUL4 E3 ligase complex, and their subsequent degradation.

Vpr causes G2/M arrest in cycling cells, but the mechanism is contentious [9, 13, 20-26], as is the connection to any replicative advantage Vpr provides *in vivo.* To investigate this important issue, we took advantage of previously characterised Vpr mutants. Residue S79 of Vpr is required for Vpr-dependent cell cycle arrest [27] (**Figure 2D** and **Figure 2 – figure supplement 1**). Of the other mutants we tested, Vpr_{Q65R} and $Vpr_{Y47A, D52A, W54R}$ mutants are also unable to cause G2/M arrest, while $Vpr_{E24R, R36P}$ has an intermediate phenotype, and Vpr_{W54R} caused G2/M arrest at wild type levels (**Figure 2D** and **Figure 2 – figure supplement 1**). Strikingly, most Vpr-dependent protein changes were also observed with the Vpr_{S79A} mutant (**Figure 2D, E**), and are therefore independent of G2/M cell cycle arrest. The presence or absence of G2/M arrest was also a poor correlate of proteomic remodelling across the entire panel of mutants. Cell cycle arrest therefore only explains a minority of Vpr-dependent changes **(Figure 2D,E)**.

Further, previous datasets/reports investigating gene and protein expression during the cell cycle have identified proteins increased or depleted during different phases of the cell cycle, or in chemically G2/M arrested cells [28, 29] (**Figure 2** – **figure supplement 4**). Cells arrested in G2 using a PLK1 inhibitor show similar regulation of the cyclin family of proteins (**Figure 2** - **figure supplement 4B**), but there is little other correlation between these datasets. Thus, whilst some changes in protein levels induced by Vpr may be explained by the effects of cell cycle arrest, proteins regulated by cell cycle in these datasets only account for a small fraction of Vpr-dependent changes (**Figure 2** - **figure supplement 4A,C,D**).

Within this minority of changes that correlate with Vpr mediated G2/M arrest, depleted proteins may either represent secondary effects of alteration to the cell cycle, or may correspond to proteins depleted by Vpr, resulting in G2/M arrest. For example, MCM10 has previously been identified as a direct target for Vpr mediated depletion, and it was also reported that depletion of MCM10 by Vpr is at least partly responsible for Vpr mediated G2/M arrest [9]. We found that depletion of MCM10

122 correlated with the degree of G2/M arrest mediated by the different Vpr variants tested in this
123 experiment (**Figure 2 – figure supplement 5A),** and confirmed that RNAi-mediated depletion of
124 MCM10 could partly phenocopy Vpr by inducing G2/M arrest, (**Figure 2 – figure supplement 5**), as
125 shown previously. Thus, a proportion of proteins whose depletion correlates with G2/M arrest in this
126 system may be causes, rather than consequences of Vpr mediated G2/M arrest.

127 **Identifying direct targets for Vpr-mediated degradation.**
128 Vpr has a nuclear localisation and all reported direct Vpr targets are nuclear proteins. Primary Vpr
129 targets are therefore predicted to be nuclear. Conversely, secondary effects resulting from, for
130 example, transcriptional changes, can be distributed across the cell. Analysis of the 302 proteins
131 depleted by Vpr revealed a profound enrichment for proteins that reside in the nucleus (>80%)
132 (**Figure 3A**). This raised the possibility that a large proportion of the proteins depleted by Vpr are
133 direct targets, as secondary effects should not be limited to the nucleus. Consistent with this,
134 proteins upregulated by Vpr, which are all predicted to be secondary effects, were distributed across
135 multiple compartments. Furthermore, proteins depleted by Vpr were enriched (>70%) for nucleic
136 acid binding activity (**Figure 3B**). Vpr associates with DNA binding proteins such as UNG via a
137 substrate-binding surface that mimics DNA [18]. Thus, rather than targeting a small number of
138 cellular proteins for degradation, Vpr may have a much wider range of direct cellular targets, and the
139 structure of the substrate binding surface suggests a possible this mechanism for recruitment of
140 multiple cellular factors.

141 To identify those proteins targeted directly by Vpr, we first adopted a co-immunoprecipitation
142 approach (**Figure 4A**). Cells were transduced with a 3xHA tagged Vpr lentivirus in the presence of an
143 shRNA to DCAF1 and the pan-cullin inhibitor MLN4924, to minimise substrate degradation and allow
144 successful co-immunoprecipitation. Factors specifically co-immunoprecipitated in the presence of
145 Vpr are expected to include direct Vpr targets and, accordingly, were enriched for proteins depleted
146 (rather than increased) in the presence of Vpr (**Figure 4B,D,E**). However, the co-IP was dominated by
147 DCAF1, a stable binding partner of Vpr, identified with a signal intensity 2 orders of magnitude
148 greater than all other proteins (**Figure 4C**). This is despite the knockdown of DCAF1 in these cells,
149 which reduces the DCAF1 protein abundance by approximately 50% (**Figure 2 – figure supplement**
150 **3B**). In addition, at least 13 of the proteins co-immunoprecipitating with Vpr are reported to
151 physically interact with DCAF1 alone [30-32], of which 11 are not regulated by Vpr, and two, CEP78
152 and IQGAP2, are upregulated by Vpr, explaining their presence in this list of proteins.

153 This mismatch between the high abundance of DCAF1 and the relatively low abundance of direct Vpr
154 targets for degradation is reminiscent of previous reports, which have also found that MS-IP based
155 techniques are ideal for the identification of the cellular machinery co-opted by viral proteins, but
156 often struggle to identify cellular targets, which interact transiently and in competition with each
157 other [33, 34]. We therefore adopted an alternative, pulsed-Stable Isotope Labelling with Amino
158 Acids in Cell Culture (pulsed-SILAC) approach to identify host proteins specifically destabilised within
159 6 hrs of exposure to Vpr (**Figure 5A**). This technique is directly analogous to a traditional pulse-chase
160 experiment using radiolabelled methionine/cysteine, but allows a global, unbiased analysis of
161 potential cellular targets [35]. Since proteins are fully labelled prior to exposure to Vpr, differences in
162 abundances of labelled proteins between conditions exclusively reflect changes in protein
163 degradation rates.

164 Six hours after exposure to Vpr, the stability of most proteins was unchanged (**Figure 5B,** top panel).
165 However, a subset of proteins depleted by Vpr were already destabilised, consistent with Vpr-
166 dependent proteasomal degradation. These 27 proteins, including HLTF, are therefore very likely to
167 represent direct targets for Vpr-mediated depletion (**Figure 5C**). After 24 hours of exposure to Vpr,
168 changes in protein stability reflected overall changes in protein abundance caused by Vpr in other
169 experiments (**Figure 5B,** lower panel), including proteins with increased as well as decreased
170 stability. These changes are therefore indicative of both direct and indirect Vpr targets.

171 Combining all our orthogonal approaches - TMT-based whole cell proteomics to identify proteins
172 depleted by Vpr in the context of viral infection or Vpr protein alone delivered in viral particles, MS
173 co-IP with epitope tagged Vpr, and pulsed-SILAC based identification of proteins post-translationally
174 degraded by Vpr - we have identified 38 direct targets for Vpr mediated degradation (**Table 1**). Vpr is
175 both necessary and sufficient for depletion of these proteins, which are either bound by Vpr, or
176 destabilised within 6 hours of Vpr exposure (or both). This list very likely underestimates the true
177 number of direct Vpr targets, as several known targets of Vpr behaved appropriately, but beyond
178 the statistical cut-offs used to derive this table (**Table 1 – table supplement 1**). It is also limited to
179 proteins expressed in this T-cell model.

180 **Novel Vpr target involvement in G2/M arrest**
181 Several cellular phenotypes have been described for Vpr, including G2/M arrest, transactivation of
182 the HIV LTR, and modulation of cellular signalling pathways such as NFκB and NFAT arrest [21, 22,
183 36-40]. The mechanisms responsible for these phenotypes are controversial. The wide-scale
184 proteome remodelling by Vpr, and the direct targeting of multiple proteins, suggests a model in
185 which Vpr interacts with diverse cellular proteins and pathways, perhaps resulting in cumulative or
186 redundant effects on cellular phenotypes. This model does not contradict any single mechanism, but
187 suggests that several are involved. To test this, we investigated the best described phenotype for
188 Vpr, cell cycle arrest at the G2/M phase. As noted, MCM10 degradation correlated with the extent of
189 G2/M arrest in the panel of Vpr mutants tested, and that RNAi for MCM10 results in G2/M arrest, as
190 previously described [9]. We therefore interrogated the Vpr mutant panel dataset (**Figure 2**) for
191 other direct targets of Vpr mediated degradation described in **Table 1** that correlated with the
192 extent of G2/M arrest. 14 proteins with a significant relationship (a linear regression analysis with p
193 < 0.05) **(Figure 6A)** were identified. We tested if their shRNA-mediated depletion could phenocopy
194 Vpr by inducing cell cycle arrest at G2/M (**Figure 6A**). Depletion of 3 Vpr targets: SMN1, CDCA2 and
195 ZNF267 caused G2/M arrest, and these phenotypes were confirmed with a second shRNA (**Figure**
196 **6C**). We suggest that depletion of multiple cellular Vpr targets contribute to the Vpr-mediated G2/M
197 arrest, consistent with our proposed model.

198 **Conservation of Vpr targets across primate lentiviruses.**
199 Targeting of key cellular proteins such as BST2 or the APOBEC3 family is conserved across multiple
200 lentiviral lineages, demonstrating the *in vivo* selective advantage of these interactions. We therefore
201 tested a diverse panel of lentiviral Vpr proteins to determine if they shared activity with the NL4-3
202 Vpr variant used in all the experiments above. We included Vpr variants from primary isolates of
203 HIV-1 from two distinct cross-species transmissions from apes to humans (Group M and Group O), in
204 addition to a closely related SIVcpz variant. We also tested Vpr variants from divergent primate
205 lineages, including HIV-2, SIVsmm, SIVagm and SIVrcm (**Figure 7A** and **Figure 7 – figure supplement**
206 **1**). In addition to Vpr, which is present in all primate lentiviruses, viruses of some lineages also bear

207 Vpx, a gene duplication of Vpr. Since depletion of some substrates switches between Vpr and Vpx in
208 lineages bearing this accessory gene, we also included a Vpx variant from HIV-2.

209 Extensive Vpr-dependent remodelling of the cellular proteome was conserved across the HIV-
210 1/SIVcpz lineage (**Figure 7B** – top row). Vpr variants from other lineages showed a narrower set of
211 changes, but the depletion of some proteins, particularly those most heavily depleted by HIV-1, was
212 conserved by Vpr variants across multiple lineages (**Figure 7B**,**C**). Depletion of selected proteins for
213 which commercial antibody reagents were available was readily confirmed by immunoblot of cells
214 transduced with an overlapping panel of Vpr variants (**Figure 7D**). Conserved targets of direct Vpr-
215 mediated degradation (highlighted in **Figure 7C** and **Figure 7 – figure supplement 1**) are therefore
216 likely to provide an *in vivo* replicative advantage for all primate lentiviruses.

217 While none of the identified HIV-1 Vpr targets were degraded by the HIV-2 Vpx (HIV-2_{ROD}) tested, we
218 noted a shared ability of HIV-2 Vpx and SIVagm Vpr to deplete TASOR, a critical component of the
219 Human Silencing Hub (HuSH) transcription repressor complex we recently described [41] (**Figure 8**).
220 The HuSH complex mediates position-dependent transcriptional repression of a subset of lentiviral
221 integrations, and antagonism of HuSH is able to potentiate HIV reactivation in the J-LAT model of
222 latency [41]. As predicted, Vpx-VLPs phenocopied the effect of RNAi-mediated TASOR depletion on
223 reactivation of the HuSH-sensitive J-LAT clone A1 (**Figure 8B**). With some exceptions, most primate
224 lentiviruses can be categorised into 5 lineages (**Figure 8C**), of which two encode Vpx. The previously
225 described canonical function of Vpx is the degradation of SAMHD1 [42, 43]. Two lentiviral lineages
226 lack Vpx, but use Vpr to degrade SAMHD1, while the HIV-1/SIVcpz lineage lacks SAMHD1 antagonism
227 [44]. We considered that TASOR antagonism may follow the same pattern, and thus tested Vpx
228 proteins from both Vpx bearing lineages, and representative Vpr variants from lineages that use Vpr
229 to degrade SAMHD1. All of these proteins were able to deplete TASOR in Vpx/Vpr transduced cells
230 (**Figure 8D**). Antagonism of SAMHD1 and TASOR therefore follow the same pattern. Whilst this
231 manuscript was in preparation, two other groups independently discovered Vpx-mediated depletion
232 of TASOR [45, 46], and the role of HuSH antagonism in lentiviral infection is the subject of ongoing
233 investigation.

234 While the targeting of some substrates was conserved across Vpr varients from multiple lineages, we
235 did not observe broad proteome remodelling outside the HIV-1/SIVcpz lineage. However, in the
236 experiment described in **Figure 7** an HIV-1 based lentiviral transduction system was used. Of the Vpr
237 and Vpx variants tested, only Vpr protein from only the HIV-1/SIVcpz alleles are efficiently packaged.
238 In these cases, cells receive both incoming and *de novo* synthesized Vpr, while in the case of other
239 variants tested, only *de novo* synthesized Vpr is present. There is therefore a time-lag of at 18-24
240 hours for viral entry, reverse transcription, integration and de novo synthesis of protein to begin. As
241 such, the more limited proteome remodelling seen in Vpr variants may reflect a lack of time for such
242 changes to occur.

243 In order to account for this, we carried out an experiment in which cells were transduced with a Vpr
244 or Vpx from the primary HIV-2 isolate 7312a and assayed 48 h to 96 hours post transduction (**Figure**
245 **9A**), allowing time for additional changes to develop after *de novo* Vpr/Vpx synthesis. Even at 96
246 hours post transduction, HIV-2 Vpr showed very limited changes. The majority of these changes
247 consisted of the depletion of proteins described above as being also targeted by HIV-1 Vpr (**Figure**
248 **9B** left panel). Widespread proteome remodelling was not observed, and global regulation of the

249 proteome is therefore unique to the HIV-1/SIVcpz lineage. As the HIV-1/SIVcpz lineage appears to
250 be more pathogenic than other primate lentiviral lineages [47, 48] this activity of HIV-1 Vpr may be
251 significant, particularly given the potential to drive these changes in Vpr exposed but uninfected
252 bystander cells.

253 Curiously, 7312a HIV-2 Vpx depleted several proteins we have identified as being modulated by HIV-
254 1 Vpr (**Figure 9B –** right panel), including direct targets for HIV-1 Vpr mediated degradation, BBX,
255 HASPIN and ARHGAP11A. Some proteins were degraded by both HIV-2 Vpr and Vpx, while others
256 were only degraded by the Vpx of this isolate. In lentiviral strains and/or lineages that encode both
257 Vpr and Vpx, responsibility for degrading key targets of HIV-1 Vpr is therefore shared between Vpr
258 and Vpx, further emphasising their *in vivo* importance.

259 Discussion

260 Proteomic analyses of cells infected with viruses from different orders have revealed widespread
261 and varied changes to the cellular proteome [5, 49-51]. While these changes are presumed to be
262 multifactorial, in the case of HIV-1 infection, the majority can be attributed to the action of a single
263 viral protein, Vpr. We propose that this massive cellular proteome remodelling consist of firstly, the
264 direct targeting of multiple cellular proteins for proteosomal degradation via the
265 DCAF1/DDB1/CUL4A E3 ligase complex, followed by resulting secondary effects on other proteins.
266 While many of the changes caused by Vpr are secondary, these changes occur within 48 hours of
267 infection or exposure to Vpr, the physiological timeframe of productively infected T-cell [52, 53], and
268 are therefore relevant to our understanding of the HIV-1 infected cell.

269 The list of direct targets for Vpr mediated depletion was already extensive. We have confirmed here
270 the Vpr mediated depletion of previously described Vpr targets HLTF [6, 7], ZGPAT [8], MCM10 [9],
271 UNG2 [10], TET2 [11], MUS81 and EME1 [12, 13], while other previously described Vpr targets
272 SMUG1 [10] and PHF13 [54] were not detected in this cell line. Based on our knowledge of the
273 activity of other HIV accessory proteins, it might have been predicted that this list of Vpr targets was
274 nearly complete. Rather, we show here that it is only the tip of the iceberg. Indeed, even with the
275 large number of direct targets identified or confirmed in this work, we do not propose that the list of
276 38 proteins identified here as direct targets here is comprehensive.

277 While surprising, the ability of Vpr to degrade multiple cellular factors can perhaps be explained by
278 elements of the biology of this small protein. Mechanistically, depletion of multiple proteins with
279 nucleic acid binding properties is consistent with known structural determinants of Vpr substrate
280 recruitment. From the functional viewpoint, while HIV-1 has three accessory proteins (Vpu, Nef and
281 Vif) to aid viral replication and counteract host defences in the late stages of the viral life cycle, Vpr is
282 the only HIV-1 accessory protein specifically packaged in virions. Multiple targets may therefore be
283 required both to protect incoming virions from cellular factors, and to prime newly infected cells for
284 productive viral replication.

285 This work does not represent the first attempt to use unbiased proteomics analysis to characterise
286 Vpr function. In general, previous studies have used one proteomics based experiment or method to
287 identify candidate proteins that either interact with, or are depleted by, Vpr, with individual proteins
288 subsequently followed up using targeted methods with immunoreagents. For example, proteins
289 identified as binding Vpr by co-immunoprecipitation MS were identified by Jager *et al* [33] and

290 Hrecka *et al* [7]. Of proteins co-immunoprecipitating with Vpr, Jager *et al* did not determine whether
291 any proteins were depleted following binding Vpr. Hrecka *et al* [7] also used an MS-IP and confirmed
292 identified the single target protein, HLTF, as depleted by Vpr, thus satisfying the criteria to be
293 identified as a Vpr target. Conversely, Lahuassa *et al* [6] used a SILAC based approach to quantify
294 protein changes in cells exposed to viral particles bearing Vpr, identifying 8 proteins which were
295 depleted by at least 20%. Of these, only one, HLTF was subsequently found to also bind Vpr, and
296 thus again by identified as a direct Vpr target. As expected, the lists of 'candidate' Vpr proteins,
297 identified, but not pursued, in the above studies overlaps with this work, and in some examples we
298 have confirmed these candidates as direct targets for Vpr mediated degradation. For example,
299 SMN1 has been identified as binding Vpr by Jager *et al*, and as being degraded by Vpr by Lahuassa *et*
300 *al* in indepenedent proteomics experiments. ESCO2 was identified as binding Vpr by Hrecka *et al,* but
301 the depletion was not confirmed by immunoblot – most likely due to poor performance of the
302 commercial antibody used. We have confirmed that both of these proteins are direct targets for Vpr
303 mediated degradation.

304 By contrast to previous studies, rather than using a targeted approach to follow up only a small
305 number of potential Vpr targets we have combined complementary proteomic analyses to describe
306 (i) the global proteome remodelling caused by Vpr, and (ii) multiple direct substrates for Vpr
307 mediated depletion. The two established criteria for Vpr targets, that Vpr both directly binds and
308 depletes a given protein are satisfied by several of the proteins identified here, including ESCO2,
309 SMN1, BBX and KIF18A. Thus, these proteins are not candidate Vpr targets, but *bone fide* Vpr
310 targets, proven to the same standard of evidence as previously described direct substrates.

311 However, in our proposed model, Vpr binds and degrades multiple cellular proteins, with the total
312 pool of Vpr shared over multiple targets. The identification of cellular targets by co-IP is thus
313 technically problematic and more prone to false negatives compared to other proteins that establish
314 interactions with a small number of binding partners. We therefore propose an alternative method
315 of identifying direct targets for Vpr mediated depletion – proteins that are post-translationally
316 degraded within 6 hours of treatment with Vpr. This strategy was more successful at capturing the
317 known effects on cellular Vpr targets than the MS-IP approach, with the degradation of HLTF and
318 ZGPAT being demonstrated within 6 hours of Vpr exposure. We are confident that the other proteins
319 identified in this fashion also represent direct targets for Vpr mediated degradation, as secondary
320 effects are excluded by both intrinsic elements of the technique, and the short time frame allowed.

321 A comparison of this work with the recent publication by Lapek *et al* [14] is required, given the major
322 differences between these studies, despite apparent similarities in the approach. Lapek *et al* use an
323 inducible HIV-1 provirus and quantify changes to the cellular proteome up to 24 hours post
324 activation. They compare a wild type and a Vpr deficient provirus but find fewer differences than in
325 this study – indeed, they identify only nine proteins with significant difference between wild type
326 and dVpr, none of which are previously defined Vpr targets – although DCAF1 is significantly reduced
327 in the presence of Vpr. The difference most likely relates to differences between the systems used.
328 In our model system, as in physiological conditions, Vpr is delivered with the virus particle at '0 h'
329 but de novo production of Vpr occurs late in the virus lifecycle. In Lapek *et al*, The experiment is
330 concluded 24 hours after induction of the provirus. As production of de novo Vpr is Rev-dependent,
331 Vpr production must occur after a significant delay within that 24-hour period. Thus, while some
332 limited primary effects are evident such as the depletion of DCAF1, other primary and secondary

333 effects may not have had time to occur. Aside from the matter of timing, it is also worth noting that
334 that in the Lapek *et al* system, all Vpr is produced concurrently with Gag. The interaction between
335 Vpr and Gag, and the recruitment of a proportion of Vpr into nascent viral particles, may inhibit
336 nuclear localisation and substrate degradation.

337 Despite the importance of Vpr *in vivo*, an *in vitro* viral replication phenotype is often absent in T-cell
338 infection models [55]. Nonetheless, expression of Vpr in T-cells causes cell cycle arrest [36-38], cell
339 death [37], transactivation of the viral LTR [36], enhancement or antagonism of crucial signalling
340 pathways including NFAT [21] and NF-κB [22, 39, 40], disruption of PARP1 localisation [21, 40],
341 defects in chromatid cohesion [56] and induction of the DNA damage response [57, 58]. At least
342 some of these phenotypes can be segregated [21, 37]. The molecular mechanisms underpinning
343 these phenomena have remained controversial. In our model, we propose that these multiple
344 phenotypes can be explained by Vpr targeting multiple cellular proteins and pathways, with
345 potential for redundant or cumulative effects.

346 Here, we have considered the most well described cellular phenotype for Vpr, G2/M cell cycle arrest,
347 with findings compatible with this model. In addition to confirming the previously described effect of
348 Vpr mediated MCM10 degradation, we have identified three other proteins that are directly
349 targeted by Vpr, show depletion correlating with the extent of G2/M mediated arrest in a panel of
350 Vpr mutants and result in arrest at G2/M when depleted through RNAi. Notably, depletion of two of
351 these proteins, SMN1 and CDCA2 (Repo-Man), has been shown to activate the DNA damage
352 response and stimulate ATM/ATR kinase activity [59, 60], demonstrated by many groups to be a
353 critical step towards the G2/M arrest caused by Vpr [20, 23, 61]. The contribution of depletion of
354 multiple cellular targets towards difference cellular phenotypes is also illustrated by another
355 example of a Vpr mediated, premature chromatid segregation (PCS). While this phenotype was not
356 investigated here, the RNAi mediated knockdown of any of three proteins we describe as novel
357 targets for Vpr mediated depletion, ESCO2, CDCA5 (Sororin) or HASPIN results in this phenotype [62-
358 64].

359 In conclusion, Vpr degrades multiple cellular targets, resulting in global remodeling of the host
360 proteome, and labyrinthine changes to different cellular pathways. This explains why its effects on
361 cellular phenotypes and viral replication are complex and remain poorly understood, why the
362 functional consequences of individual Vpr targets identified and studied in isolation have proved
363 elusive, and why the search for a single, critical Vpr target has been problematic.

364 Acknowledgements

365 This work was supported by the Wellcome Trust (PRF 101835/Z/13/Z to PJL), the MRC (CSF
366 MR/P008801/1 to NJM), NHSBT (WPA15-02 to NJM), the NIHR Cambridge BRC, and a Wellcome
367 Trust Strategic Award to the CIMR. The authors thank Dr. Reiner Schulte and the CIMR Flow
368 Cytometry Core Facility team, and the Lehner laboratory for critical discussion.

369 Data availability

370 In addition to **Figure 1—source data 1**, which includes data from all of the proteomics experiments
371 carried out here, proteomics data have been deposited to the ProteomeXchange Consortium via the
372 PRIDE [65] partner repository with the dataset identifier PXD01029.

373 ## Experimental Procedures

374 **NL4-3 molecular clones**

375 pNL4-3-dE-EGFP (derived from the HIV-1 molecular clone pNL4-3 but encoding Enhanced Green
376 Fluorescent Protein (EGFP) in the *env* open reading frame (ORF), rendering Env non-functional) was
377 obtained through the AIDS Reagent Program, Division of AIDS, NIAD, NIH: Drs Haili Zhang, Yan Zhou,
378 and Robert Siliciano [66] and the complete sequence verified by Sanger sequencing. The ΔVpr
379 mutant was generated by cloning three stop codons into the Vpr open reading frame, immediately
380 after the overlap with Vif to prevent interference with that gene:
381 WT Vpr ORF sequence
382 ATGGAACAAGCCCCAGAAGACCAAGGGCCACAGAGGGAGCCATACAATGAATGGACACTAGAGCTTTTAGAGGAA
383 ΔVpr ORF sequence
384 ATGGAACAAGCCCCAGAAGACCAAGGGCCACAGAGGGAGCCATACAATGAATGGACACTAGAGCTTTAATAGTAA

385 **Viral stocks**

386 VSVg-pseudotyped NL4-3-dE-EGFP HIV viral stocks were generated by co-transfection with pMD.G
387 (VSVg) as previously described[5]. NL4-3-dE-EGFP HIV viral stocks were titred by
388 infection/transduction of known numbers of relevant target cells under standard experimental
389 conditions followed by flow cytometry for GFP and CD4 at 48 hr to identify % infected cells.
390 Single Vpr and Vpx proteins were expressed in a modified dual promotor pHRSIN[67] vector in
391 which Vpr or Vpx expression is driven by the rous sarcoma virus (RSV) promotor, and Emerald GFP
392 expression is driven by the ubiquitin promotor. Virus was generated by co-transfection with p8.91
393 and pMD.G in 293T as previously described[5]. Infectious MOI was normalised by infection in the
394 absence of reverse transcription (RTi) inhibitors, which were included where specified (see below).
395 The panel of Vpr and Vpr proteins used are detailed in **Table 2**. Amino acid sequences were codon
396 optimized and synthesized as double stranded DNA (IDT), inserted into the empty vector construct
397 by Gibson assembly, and confirmed by sanger sequencing.

398 **CEM-T4 T-cell infections**

399 CEM-T4 T-cells were infected with concentrated NL4-3-dE-EGFP or pHRSIN lentiviral stocks by
400 spinoculation at 800 ×g for 1 h in a non-refrigerated benchtop centrifuge in complete media
401 supplemented with 10 mM HEPES. Where reverse transcription treatment was specified (RTi), cells
402 were incubated with zidovudine (10 µM) and efavirenz (100 nM) (AIDS Reagent Program, Division of
403 AIDS, NIAD, NIH) for 1 hr prior to spinoculation, and inhibitors maintained at these concentrations
404 during subsequent cell culture. For MS experiments, cells were subject to dead cell removal
405 (magnetic dead cell removal kit, Miltenyi). Subsequent sample preparation, TMT labelling, and MS
406 are described below, at the end of this section.

407 **Pulsed Stable isotope labelling with amino acids in cell culture (Pulsed-SILAC)**

408 For SILAC labelling, CEM-T4 T-cells were grown for at least 7 cell divisions in SILAC RPMI lacking
409 lysine and arginine (Thermo Scientific, Thermo Fisher Scientific, UK) supplemented with 10% dialysed
410 FCS (Gibco, Thermo Fisher Scientific), 100 units/ml penicillin and 0.1 mg/ml streptomycin, 280 mg/L
411 proline (Sigma, UK) and medium (K4, R6; Cambridge Isotope Laboratories, Tewksbury, MA) or heavy
412 (K8, R10; Cambridge Isotope Laboratories) $^{13}C/^{15}N$-containing lysine (K) and arginine (R) at 50 mg/L.
413 At 0 h, cells were washed in media containing only light (^{12}C /^{14}N) lysine and arginine and were

414 maintained in this media for the duration of the experiment. Additional detail on MS methods is
415 available at the end of this section.

416 **Lentivector for shRNA expression**

417 For lentiviral shRNA-mediated knockdown of DCAF1 hairpins were cloned into pHRSIREN-PGK-hygro,
418 with transduced cells selected for hygromycin resistance.
419 The following oligonucleotide was inserted using BamHI-EcoRI (only top oligonucleotide shown),
420 identified from the Broad Institute GPP Web portal. Gene specific target sequence (forward and
421 reverse complement) is underlined.

422 **DCAF1**

423 GATCCGCTGAGAATACTCTTCAAGAATTCAAGAGATTCTTGAAGAGTATTCTCAGCTTTTTTG

424 The same methodology was used to clone other shRNA haripins, the forward orientation targeting
425 sequence used for each is shown below.

MCM10-1

AGATGCAGGAGCGCTACTTTG

MCM10-2

GACGGCGACGGTGAATCTTAT

CCNT1

GCCTGCATTTGACCACATTTA

PINX1

CCTTCAGCAAGAGAGTTTAAT

ZNF267-1

TACTCGTTCCTCCAATCTTAT

ZNF267-2

ATCAATATAGGAAGGTCTTTA

MBD1

CACCAACCTTCCAAGTGTAAA

KIF20A

CCGATGACGATGTCGTAGTTT

CWC25

GATCACAGAAGAAGATGGCA

CDCA5

CGAGAAACAGAAACGTAAGAA

ZNF574

ACCACCTTGTAAGTTCTAAAT

SMN1-1

ATCTGTGAAGTAGCTAATAA

SMN1-2

GGCTATCATACTGGCTATTAT

CDCA2 -1

AGACTGGGTTCAGGTTATTTC

CDCA2 -2

CCGTTCTCAGTTCTCCTAATA

DDX20

TCAGCTACTTATCCCGAATTT

ZNF316

CTTCCAAAGTGCTGGGATTAT

MSH6

AGGCGAAGTAGCCGCCAAATA

RFC1

CGCACTAATTATCAAGCTTAT

426 **Mass spectrometry Immunoprecipitation (MS-IP)**

427 CEM-T4 T-cells were lysed in 1 % NP-40. Lysates were pre-cleared with IgG-Sepharose (GE
428 Healthcare, UK) and incubated for 3 hr at 4°C with anti-HA coupled to agarose beads (Sigma EZview
429 Red Anti-HA Affinity Gel). After washing in 0.5% NP-40, samples were eluted with 0.5 mg/ml HA
430 peptide at 37°C for 1 hr. Additional detail on MS methods is available at the end of this section.

431 Proteins defined as co-immunoprecipitating with Vpr were detected with at least 3 peptides in the
432 Vpr condition, not identified in the control condition, and were present in <20% of MS-IP available in
433 the Crapome [68] database http://crapome.org/.

434 **Antibodies**

435 Antibodies against the following proteins were used for immunoblot, listed by manufacturer: Atlas
436 antibodies: TASOR (HPA006735). Bethyl: BBX (A303-151A), HLTF (A300-230A), RALY (A302-070A),
437 ZNF512B (A303-234A). Cell signalling : SMN1/2 (2F1). Novus: ESCO2 (NB100-87021). Origine: UNG2
438 (2C12). Proteintech: Vpr (51143-I-AP). Santa Cruz: CCNB1 (SC-245), ZGPAT (SC-51524). Sigma: β-actin
439 (AC74). Abcam : p24 (ab9071), VCP (ab11433). The following secondary antibodies were used: goat
440 anti-mouse-HRP and anti-rabbit-HRP (immunoblot, Jackson ImmunoResearch, West Grove, PA). Anti-
441 CD4-AF647 (clone OKT4; BioLegend) and anti-CD271 (NGFR)-APC (clone ME20.4, Biolegend) were
442 used for flow cytometry.

443 **J-LAT reactivation experiments.**

444 JLAT A1 cells were transduced with Cre recombinase, NL4-3 Vpr or HIV-2 ROD Vpx within a pHRSIN
445 IRES NGFR vector[69]. 24 h after transduction, cells were treated with 2 ng/ml TNFα (PeproTech,
446 300-01A). After an additional 24 h cells were stained with anti-NGFR APC and analysed for APC and
447 GFP expression by flow cytometry. Cells were gated for NGFR+ cells to exclude non-transduced cells.
448 Flow cytometry data was acquired on a BD FACSCalibur.

449 **Statistical analysis**

450 Anova and Fisher's exact test analysis were carried out as described in figure legends using
451 Graphpad Prism (v7.04). TMT multiplexed proteomics datasets were analysed using a moderated T-
452 test analysis with Benjamini-Hochberg correction [70], carried out using R (v3.3.1) [71]. Significance
453 B values for pulsed-SILAC analysis were calculated using Perseus [72].

454 **Gene ontology enrichment analysis**

455 Analysis was carried out using Panther [73], using the web interface at: http://pantherdb.org/. Lists
456 of proteins highly significantly depleted or increased by Vpr were compared to a background list of
457 proteins quantified in the two experiments used to define those lists.

458 **7-AAD staining**

459 Cells were fixed in ice cold 70% ethanol for at least 30 minutes, washed with PBS and stained in
460 25ug/ml 7-AAD for 15 minutes before acquisition on a BD FACSCalibur. Analysis was carried out in
461 Flowjo, v.10.5.2. Dead cells and doublets were excluded by gating on forward scatter, side scatter,
462 and fluorescent area and height. Univariate cell cycle modelling was carried out using the Watson
463 pragmatic method.

464 **ShRNA knockdown confirmation by RT-PCR**

465 Total RNA was extracted using the RNeasy Plus Mini kit (Qiagen). Total RNA (250 ng) was reverse
466 transcribed into cDNA using a poly(d)T primers and SuperScript III Reverse Transcriptase (Invitrogen)
467 following the manufacturer's instructions. Real-time qRT–PCR was performed using the ABI 7500
468 Real-Time PCR system (Applied Biosystems) and SYBR Green PCR Master Mix (Applied Biosystems),
469 with cycling parameters of 50°C for 2 min and 95°C for 5 min, followed by 40 cycles of 95°C for 15 s

470 and 60°C for 1 min. The gene-of-interest specific primer pairs were predesigned and purchased from
471 Sigma-Aldrich as KiCqStart primers, with the following sequences: MCM10_FOR 5'-
472 CTTATACAGAAGAGGCTGATG and MCM10_REV 5'-CCTCTTGCAACTCTTCATTC; ZNF267_FOR 5'-
473 GTAGAATTCTCTTTGGAGGAG and ZNF267_REV 5'-CTCACTCTTCACATTCCAAG; CDCA2_FOR 5'-
474 AGGAAAGTCATCATCCTACC and CDCA2_REV 5'-GATGGTTTGTTTCAGGAGAG; SMN1_FOR 5'-
475 GGAAAGCCAGGTCTAAAATTC and SMN1_REV 5'-AGAATCTGGACATATGGGAG. The difference in the
476 amount of input cDNA was normalized to an internal control of GAPDH, using the following primers:
477 GAPDH_FOR: 5' ATGGGGAAGGTGAAGGTCG and GAPDH_REV: 5'- CTCCACGACGTACTCAGCG.

478 **Phylogenetic tree of Vpr sequences.**

479 An existing nucleic acid sequence alignment of 191 representative Vif sequences from HIV-1, HIV-2
480 and SIVs from 22 primate species was downloaded from:

481 https://www.hiv.lanl.gov/content/sequence/NEWALIGN/align.html

482 A tree was generated using the percentage identity average distance in jalview [74] and visualised in
483 Figtree:

484 http://tree.bio.ed.ac.uk/software/figtree/

485 10 sequences from 5 primate species not falling into the 5 highlighted linages are not shown.

486 **Sample Preparation for Mass spectrometry**

487 Samples were prepared using three different methods depending on the experiment. Initial infection
488 experiment was by SDC-FASP. VLP and shRNA experiments were by PreOmics NHS-iST sample
489 preparation Kit. pSILAC and MS-IP experiments were by SP3.

490 *SDC-FASP*

491 Samples prepared essentially according to the protocol in Leon *et al*[75]. Briefly samples were lysed
492 in 50mM TEAB (pH8.5) 2% SDS, reduced and alkylated with TCEP/Iodoacetamide, quantified by BCA
493 assay. 50ug of each sample was diluted with TEAB/8M urea for loading onto 30kDa ultrafiltration
494 devices. Samples were washed 3 times with 500uL urea buffer and 3 times with digestion buffer
495 (TEAB/0.5% sodium deoxycholate) before resuspending in 50uL digestion buffer containing 1ug
496 trypsin and incubating overnight at 37 degrees. After digestion samples were spun through the filters
497 and filters washed with 50uL TEAB. SDC was removed by acidification and two phase partitioning with
498 ethyl acetate before vacuum drying and labelling with TMT reagents according to the manufacturer's
499 instructions.

500 *PreOmics iST*

501 Samples lysed in kit lysis buffer and quantified by BCA assay. 25ug of each sample was digested
502 essentially according to manufacturer's instructions, scaling volumes for a digestion of 25ug total
503 protein.

504 *SP3*

505 Samples were lysed in 50mM TEAB (pH8.5) 2% SDS (MS-IPs were adjusted to 2% SDS), reduced and
506 alkylated with TCEP/Iodoacetamide before digestion using the SP3 method[76]. Briefly, carboxylate
507 modified paramagnetic beads are added to the sample and protein is bound to the beads by
508 acidification with formic acid and addition of acetonitrile (ACN, final 50%). The beads are then washed
509 sequentially with 100% ACN, 70% Ethanol (twice) and 100% ACN. 10-20uL TEAB (Triethylammonium

510 bicarbonate) pH8 and 0.1% Sodium deoxycholate (SDC) is then added to the washed beads along with
511 trypsin. Samples were then incubated overnight at 37 degrees with periodic shaking at 2000rpm. After
512 digestion, peptides are immobilised on beads by addition of 200-400uL ACN and washed twice with
513 100uL ACN before eluting in 19uL 2% DMSO and removing the eluted peptide from the beads.

514 **Off-line high pH reversed-phase (HpRP) peptide fractionation**

515 For whole cell proteome samples HpRP fractionation was conducted on an Ultimate 3000 UHPLC
516 system (Thermo Scientific) equipped with a 2.1 mm × 15 cm, 1.7µ Aqcuity BEH C18 column (Waters,
517 UK). Solvent A was 3% ACN, Solvent B was 100% ACN, solvent C was 200 mM ammonium formate (pH
518 10). Throughout the analysis solvent C was kept at a constant 10%. The flow rate was 400 µL/min and
519 UV was monitored at 280 nm. Samples were loaded in 90% A for 10 min before a gradient elution of
520 0–10% B over 10 min (curve 3), 10-34% B over 21 min (curve 5), 34-50% B over 5 mins (curve 5)
521 followed by a 10 min wash with 90% B. 15 s (100 µL) fractions were collected throughout the run.
522 Peptide containing fractions were orthogonally recombined into 24 fractions (i.e. fractions 1, 25, 49,
523 73, 97 combined) and dried in a vacuum centrifuge. Fractions were stored at −80°C prior to analysis.

524 **Mass spectrometry**

525 Data were acquired on an Orbitrap Fusion mass spectrometer (Thermo Scientific) coupled to an
526 Ultimate 3000 RSLC nano UHPLC (Thermo Scientific). HpRP fractions were resuspended in 20 µl 5%
527 DMSO 0.5% TFA and 10uL injected. Fractions were loaded at 10 µl/min for 5 min on to an Acclaim
528 PepMap C18 cartridge trap column (300 um × 5 mm, 5 um particle size) in 0.1% TFA. After loading a
529 linear gradient of 3–32% solvent B was used for sample separation over a column of the same
530 stationary phase (75 µm × 50 cm, 2 µm particle size) before washing at 90% B and re-equilibration.
531 Solvents were A: 0.1% FA and B:ACN/0.1% FA. 3h gradients were used for whole cell proteomics
532 samples, 1h gradients for MS-IPs.

533 An SPS/MS3 acquisition was used for TMT experiments and was run as follows. MS1: Quadrupole
534 isolation, 120’000 resolution, 5e5 AGC target, 50 ms maximum injection time, ions injected for all
535 parallelisable time. MS2: Quadrupole isolation at an isolation width of m/z 0.7, CID fragmentation
536 (NCE 35) with the ion trap scanning out in rapid mode from m/z 120, 8e3 AGC target, 70 ms maximum
537 injection time, ions accumulated for all parallelisable time. In synchronous precursor selection mode
538 the top 10 MS2 ions were selected for HCD fragmentation (65NCE) and scanned out in the orbitrap at
539 50’000 resolution with an AGC target of 2e4 and a maximum accumulation time of 120 ms, ions were
540 not accumulated for all parallelisable time. The entire MS/MS/MS cycle had a target time of 3 s.
541 Dynamic exclusion was set to +/−10 ppm for 90 s, MS2 fragmentation was trigged on precursor ions
542 5e3 counts and above. For MS-IPs, MS2 instead used HCD fragmentation (NCE 34) and a maximum
543 injection time of 250ms and had a target cycle time of 2s. For pSILAC MS1 was acquired at 240’000
544 resolution.

545 **Data processing and analysis**

546 For TMT labelled samples data were searched by Mascot within Proteome Discoverer 2.1 in two
547 rounds of searching. First search was against the UniProt Human reference proteome (26/09/17), the
548 HIV proteome and compendium of common contaminants (GPM). The second search took all
549 unmatched spectra from the first search and searched against the human trEMBL database (Uniprot,
550 26/09/17). The following search parameters were used. MS1 Tol: 10 ppm, MS2 Tol: 0.6 Da. Enzyme:

551 Trypsin (/P). MS3 spectra were used for reporter ion based quantitation with a most confident
552 centroid tolerance of 20 ppm. PSM FDR was calculated using Mascot percolator and was controlled at
553 0.01% for 'high' confidence PSMs and 0.05% for 'medium' confidence PSMs. Normalisation was
554 automated and based on total s/n in each channel. Protein/peptide abundance was calculated and
555 output in terms of 'scaled' values, where the total s/n across all reporter channels is calculated and a
556 normalised contribution of each channel is output. Proteins/peptides satisfying at least a 'medium'
557 FDR confidence were taken forth to statistical analysis in R. This consisted of a moderated T-test
558 (Limma) with Benjamini-Hochberg correction for multiple hypotheses to provide a q value for each
559 comparison [70]. MS-IPs were submitted to a similar search workflow with quantitative data being
560 derived from MS1 spectra via proteome discover minora feature detector node. For pSILAC
561 experiments data were processed in MaxQuant and searched using Andromeda with similar search
562 parameters [77]. MaxQuant output was uploaded into Perseus for calculation of significance B [72].
563 Where conditions were not carried out in triplicate, downstream analysis was limited to proteins
564 identified with at least 3 unique peptides.

565 **References**

566 1. Matheson, N.J., E.J. Greenwood, and P.J. Lehner, *Manipulation of immunometabolism by*
567 *HIV-accessories to the crime?* Curr Opin Virol, 2016. **19**: p. 65-70.
568 2. Sugden, S.M., et al., *Remodeling of the Host Cell Plasma Membrane by HIV-1 Nef and Vpu: A*
569 *Strategy to Ensure Viral Fitness and Persistence.* Viruses, 2016. **8**(3).
570 3. Simon, V., N. Bloch, and N.R. Landau, *Intrinsic host restrictions to HIV-1 and mechanisms of*
571 *viral escape.* Nat Immunol, 2015. **16**(6): p. 546-53.
572 4. Matheson, N.J., et al., *Cell Surface Proteomic Map of HIV Infection Reveals Antagonism of*
573 *Amino Acid Metabolism by Vpu and Nef.* Cell Host Microbe, 2015. **18**(4): p. 409-23.
574 5. Greenwood, E.J., et al., *Temporal proteomic analysis of HIV infection reveals remodelling of*
575 *the host phosphoproteome by lentiviral Vif variants.* Elife, 2016. **5**.
576 6. Lahouassa, H., et al., *HIV-1 Vpr degrades the HLTF DNA translocase in T cells and*
577 *macrophages.* Proc Natl Acad Sci U S A, 2016.
578 7. Hrecka, K., et al., *HIV-1 and HIV-2 exhibit divergent interactions with HLTF and UNG2 DNA*
579 *repair proteins.* Proc Natl Acad Sci U S A, 2016. **113**(27): p. E3921-30.
580 8. Maudet, C., et al., *HIV-1 Vpr induces the degradation of ZIP and sZIP, adaptors of the NuRD*
581 *chromatin remodeling complex, by hijacking DCAF1/VprBP.* PLoS One, 2013. **8**(10): p.
582 e77320.
583 9. Romani, B., et al., *HIV-1 Vpr Protein Enhances Proteasomal Degradation of MCM10 DNA*
584 *Replication Factor through the Cul4-DDB1[VprBP] E3 Ubiquitin Ligase to Induce G2/M Cell*
585 *Cycle Arrest.* J Biol Chem, 2015. **290**(28): p. 17380-9.
586 10. Schrofelbauer, B., et al., *Human immunodeficiency virus type 1 Vpr induces the degradation*
587 *of the UNG and SMUG uracil-DNA glycosylases.* J Virol, 2005. **79**(17): p. 10978-87.
588 11. Lv, L., et al., *Vpr Targets TET2 for Degradation by CRL4(VprBP) E3 Ligase to Sustain IL-6*
589 *Expression and Enhance HIV-1 Replication.* Mol Cell, 2018. **70**(5): p. 961-970 e5.
590 12. Zhou, X., M. DeLucia, and J. Ahn, *SLX4-SLX1 Protein-independent Down-regulation of MUS81-*
591 *EME1 Protein by HIV-1 Viral Protein R (Vpr).* J Biol Chem, 2016. **291**(33): p. 16936-16947.
592 13. Laguette, N., et al., *Premature activation of the SLX4 complex by Vpr promotes G2/M arrest*
593 *and escape from innate immune sensing.* Cell, 2014. **156**(1-2): p. 134-45.
594 14. Lapek, J.D., Jr., et al., *Quantitative Temporal Viromics of an Inducible HIV-1 Model Yields*
595 *Insight to Global Host Targets and Phospho-Dynamics Associated with Protein Vpr.* Mol Cell
596 Proteomics, 2017. **16**(8): p. 1447-1461.
597 15. Goh, W.C., et al., *HIV-1 Vpr increases viral expression by manipulation of the cell cycle: a*
598 *mechanism for selection of Vpr in vivo.* Nat Med, 1998. **4**(1): p. 65-71.

599 16. Forget, J., et al., *Human immunodeficiency virus type 1 vpr protein transactivation function:*
600 *mechanism and identification of domains involved.* J Mol Biol, 1998. **284**(4): p. 915-23.
601 17. Le Rouzic, E., et al., *HIV1 Vpr arrests the cell cycle by recruiting DCAF1/VprBP, a receptor of*
602 *the Cul4-DDB1 ubiquitin ligase.* Cell Cycle, 2007. **6**(2): p. 182-8.
603 18. Wu, Y., et al., *The DDB1-DCAF1-Vpr-UNG2 crystal structure reveals how HIV-1 Vpr steers*
604 *human UNG2 toward destruction.* Nat Struct Mol Biol, 2016. **23**(10): p. 933-940.
605 19. Selig, L., et al., *Uracil DNA glycosylase specifically interacts with Vpr of both human*
606 *immunodeficiency virus type 1 and simian immunodeficiency virus of sooty mangabeys, but*
607 *binding does not correlate with cell cycle arrest.* J Virol, 1997. **71**(6): p. 4842-6.
608 20. Fregoso, O.I. and M. Emerman, *Activation of the DNA Damage Response Is a Conserved*
609 *Function of HIV-1 and HIV-2 Vpr That Is Independent of SLX4 Recruitment.* MBio, 2016. **7**(5).
610 21. Hohne, K., et al., *Virion encapsidated HIV-1 Vpr induces NFAT to prime non-activated T cells*
611 *for productive infection.* Open Biol, 2016. **6**(7).
612 22. Liang, Z., et al., *HIV-1 Vpr protein activates the NF-kappaB pathway to promote G2/M cell*
613 *cycle arrest.* Virol Sin, 2015. **30**(6): p. 441-8.
614 23. Berger, G., et al., *G2/M cell cycle arrest correlates with primate lentiviral Vpr interaction with*
615 *the SLX4 complex.* J Virol, 2015. **89**(1): p. 230-40.
616 24. Belzile, J.P., et al., *HIV-1 Vpr induces the K48-linked polyubiquitination and proteasomal*
617 *degradation of target cellular proteins to activate ATR and promote G2 arrest.* J Virol, 2010.
618 **84**(7): p. 3320-30.
619 25. Terada, Y. and Y. Yasuda, *Human immunodeficiency virus type 1 Vpr induces G2 checkpoint*
620 *activation by interacting with the splicing factor SAP145.* Mol Cell Biol, 2006. **26**(21): p. 8149-
621 58.
622 26. Re, F., et al., *Human immunodeficiency virus type 1 Vpr arrests the cell cycle in G2 by*
623 *inhibiting the activation of p34cdc2-cyclin B.* J Virol, 1995. **69**(11): p. 6859-64.
624 27. Zhou, Y. and L. Ratner, *Phosphorylation of human immunodeficiency virus type 1 Vpr*
625 *regulates cell cycle arrest.* J Virol, 2000. **74**(14): p. 6520-7.
626 28. Fischer, M., et al., *Integration of TP53, DREAM, MMB-FOXM1 and RB-E2F target gene*
627 *analyses identifies cell cycle gene regulatory networks.* Nucleic Acids Res, 2016. **44**(13): p.
628 6070-86.
629 29. Ly, T., A. Endo, and A.I. Lamond, *Proteomic analysis of the response to cell cycle arrests in*
630 *human myeloid leukemia cells.* Elife, 2015. **4**.
631 30. Hossain, D., et al., *Cep78 controls centrosome homeostasis by inhibiting EDD-DYRK2-*
632 *DDB1(Vpr)(BP).* EMBO Rep, 2017. **18**(4): p. 632-644.
633 31. Coyaud, E., et al., *Global Interactomics Uncovers Extensive Organellar Targeting by Zika*
634 *Virus.* Mol Cell Proteomics, 2018. **17**(11): p. 2242-2255.
635 32. Guo, Z., et al., *DCAF1 controls T-cell function via p53-dependent and -independent*
636 *mechanisms.* Nat Commun, 2016. **7**: p. 10307.
637 33. Jager, S., et al., *Global landscape of HIV-human protein complexes.* Nature, 2011. **481**(7381):
638 p. 365-70.
639 34. Luo, Y., et al., *HIV-host interactome revealed directly from infected cells.* Nat Microbiol, 2016.
640 **1**(7): p. 16068.
641 35. Boisvert, F.M., et al., *A quantitative spatial proteomics analysis of proteome turnover in*
642 *human cells.* Mol Cell Proteomics, 2012. **11**(3): p. M111 011429.
643 36. Gummuluru, S. and M. Emerman, *Cell cycle- and Vpr-mediated regulation of human*
644 *immunodeficiency virus type 1 expression in primary and transformed T-cell lines.* J Virol,
645 1999. **73**(7): p. 5422-30.
646 37. Bolton, D.L. and M.J. Lenardo, *Vpr cytopathicity independent of G2/M cell cycle arrest in*
647 *human immunodeficiency virus type 1-infected CD4+ T cells.* J Virol, 2007. **81**(17): p. 8878-90.
648 38. Rogel, M.E., L.I. Wu, and M. Emerman, *The human immunodeficiency virus type 1 vpr gene*
649 *prevents cell proliferation during chronic infection.* J Virol, 1995. **69**(2): p. 882-8.

650 39. Liu, R., et al., *HIV-1 Vpr stimulates NF-kappaB and AP-1 signaling by activating TAK1.*
651 Retrovirology, 2014. **11**: p. 45.
652 40. Muthumani, K., et al., *The HIV-1 Vpr and glucocorticoid receptor complex is a gain-of-*
653 *function interaction that prevents the nuclear localization of PARP-1.* Nat Cell Biol, 2006.
654 **8**(2): p. 170-9.
655 41. Tchasovnikarova, I.A., et al., *GENE SILENCING. Epigenetic silencing by the HUSH complex*
656 *mediates position-effect variegation in human cells.* Science, 2015. **348**(6242): p. 1481-1485.
657 42. Hrecka, K., et al., *Vpx relieves inhibition of HIV-1 infection of macrophages mediated by the*
658 *SAMHD1 protein.* Nature, 2011. **474**(7353): p. 658-61.
659 43. Laguette, N., et al., *SAMHD1 is the dendritic- and myeloid-cell-specific HIV-1 restriction factor*
660 *counteracted by Vpx.* Nature, 2011. **474**(7353): p. 654-7.
661 44. Lim, E.S., et al., *The ability of primate lentiviruses to degrade the monocyte restriction factor*
662 *SAMHD1 preceded the birth of the viral accessory protein Vpx.* Cell Host Microbe, 2012.
663 **11**(2): p. 194-204.
664 45. Chougui, G., et al., *HIV-2/SIV viral protein X counteracts HUSH repressor complex.* Nat
665 Microbiol, 2018.
666 46. Yurkovetskiy, L., et al., *Primate immunodeficiency virus proteins Vpx and Vpr counteract*
667 *transcriptional repression of proviruses by the HUSH complex.* Nat Microbiol, 2018.
668 47. Greenwood, E.J., et al., *Simian Immunodeficiency Virus Infection of Chimpanzees (Pan*
669 *troglodytes) Shares Features of Both Pathogenic and Non-pathogenic Lentiviral Infections.*
670 PLoS Pathog, 2015. **11**(9): p. e1005146.
671 48. Keele, B.F., et al., *Increased mortality and AIDS-like immunopathology in wild chimpanzees*
672 *infected with SIVcpz.* Nature, 2009. **460**(7254): p. 515-9.
673 49. Ersing, I., et al., *A Temporal Proteomic Map of Epstein-Barr Virus Lytic Replication in B Cells.*
674 Cell Rep, 2017. **19**(7): p. 1479-1493.
675 50. Weekes, M.P., et al., *Quantitative temporal viromics: an approach to investigate host-*
676 *pathogen interaction.* Cell, 2014. **157**(6): p. 1460-72.
677 51. Diamond, D.L., et al., *Temporal proteome and lipidome profiles reveal hepatitis C virus-*
678 *associated reprogramming of hepatocellular metabolism and bioenergetics.* PLoS Pathog,
679 2010. **6**(1): p. e1000719.
680 52. Murray, J.M., A.D. Kelleher, and D.A. Cooper, *Timing of the components of the HIV life cycle*
681 *in productively infected CD4+ T cells in a population of HIV-infected individuals.* J Virol, 2011.
682 **85**(20): p. 10798-805.
683 53. Perelson, A.S., et al., *HIV-1 dynamics in vivo: virion clearance rate, infected cell life-span, and*
684 *viral generation time.* Science, 1996. **271**(5255): p. 1582-6.
685 54. Hofmann, S., et al., *Dual role of the chromatin-binding factor PHF13 in the pre- and post-*
686 *integration phases of HIV-1 replication.* Open Biol, 2017. **7**(10).
687 55. Guenzel, C.A., C. Herate, and S. Benichou, *HIV-1 Vpr-a still "enigmatic multitasker".* Front
688 Microbiol, 2014. **5**: p. 127.
689 56. Shimura, M., et al., *Epigenetic displacement of HP1 from heterochromatin by HIV-1 Vpr*
690 *causes premature sister chromatid separation.* J Cell Biol, 2011. **194**(5): p. 721-35.
691 57. Vassena, L., et al., *The human immunodeficiency virus type 1 Vpr protein upregulates PVR via*
692 *activation of the ATR-mediated DNA damage response pathway.* J Gen Virol, 2013. **94**(Pt 12):
693 p. 2664-9.
694 58. Richard, J., et al., *HIV-1 Vpr up-regulates expression of ligands for the activating NKG2D*
695 *receptor and promotes NK cell-mediated killing.* Blood, 2010. **115**(7): p. 1354-63.
696 59. Kannan, A., et al., *Combined deficiency of Senataxin and DNA-PKcs causes DNA damage*
697 *accumulation and neurodegeneration in spinal muscular atrophy.* Nucleic Acids Res, 2018.
698 **46**(16): p. 8326-8346.
699 60. Peng, A., et al., *Repo-man controls a protein phosphatase 1-dependent threshold for DNA*
700 *damage checkpoint activation.* Curr Biol, 2010. **20**(5): p. 387-96.

701 61. Roshal, M., et al., *Activation of the ATR-mediated DNA damage response by the HIV-1 viral*
702 *protein R.* J Biol Chem, 2003. **278**(28): p. 25879-86.
703 62. Hou, F. and H. Zou, *Two human orthologues of Eco1/Ctf7 acetyltransferases are both*
704 *required for proper sister-chromatid cohesion.* Mol Biol Cell, 2005. **16**(8): p. 3908-18.
705 63. Dai, J., B.A. Sullivan, and J.M. Higgins, *Regulation of mitotic chromosome cohesion by Haspin*
706 *and Aurora B.* Dev Cell, 2006. **11**(5): p. 741-50.
707 64. Rankin, S., N.G. Ayad, and M.W. Kirschner, *Sororin, a substrate of the anaphase-promoting*
708 *complex, is required for sister chromatid cohesion in vertebrates.* Mol Cell, 2005. **18**(2): p.
709 185-200.
710 65. Vizcaino, J.A., et al., *2016 update of the PRIDE database and its related tools.* Nucleic Acids
711 Res, 2016. **44**(22): p. 11033.
712 66. Zhang, H., et al., *Novel single-cell-level phenotypic assay for residual drug susceptibility and*
713 *reduced replication capacity of drug-resistant human immunodeficiency virus type 1.* J Virol,
714 2004. **78**(4): p. 1718-29.
715 67. van den Boomen, D.J., et al., *TMEM129 is a Derlin-1 associated ERAD E3 ligase essential for*
716 *virus-induced degradation of MHC-I.* Proc Natl Acad Sci U S A, 2014. **111**(31): p. 11425-30.
717 68. Mellacheruvu, D., et al., *The CRAPome: a contaminant repository for affinity purification-*
718 *mass spectrometry data.* Nat Methods, 2013. **10**(8): p. 730-6.
719 69. Matheson, N.J., A.A. Peden, and P.J. Lehner, *Antibody-free magnetic cell sorting of*
720 *genetically modified primary human CD4+ T cells by one-step streptavidin affinity*
721 *purification.* PLoS One, 2014. **9**(10): p. e111437.
722 70. Schwammle, V., I.R. Leon, and O.N. Jensen, *Assessment and improvement of statistical tools*
723 *for comparative proteomics analysis of sparse data sets with few experimental replicates.* J
724 Proteome Res, 2013. **12**(9): p. 3874-83.
725 71. R Core Team, *R: A language and environment for statistical computing.* Vienna, Austria.
726 http://www.R-project.org/. 2013.
727 72. Tyanova, S., et al., *The Perseus computational platform for comprehensive analysis of*
728 *(prote)omics data.* Nat Methods, 2016. **13**(9): p. 731-40.
729 73. Mi, H., et al., *PANTHER version 11: expanded annotation data from Gene Ontology and*
730 *Reactome pathways, and data analysis tool enhancements.* Nucleic Acids Res, 2017. **45**(D1):
731 p. D183-D189.
732 74. Waterhouse, A.M., et al., *Jalview Version 2--a multiple sequence alignment editor and*
733 *analysis workbench.* Bioinformatics, 2009. **25**(9): p. 1189-91.
734 75. Leon, I.R., et al., *Quantitative assessment of in-solution digestion efficiency identifies optimal*
735 *protocols for unbiased protein analysis.* Mol Cell Proteomics, 2013. **12**(10): p. 2992-3005.
736 76. Hughes, C.S., et al., *Ultrasensitive proteome analysis using paramagnetic bead technology.*
737 Mol Syst Biol, 2014. **10**: p. 757.
738 77. Cox, J. and M. Mann, *MaxQuant enables high peptide identification rates, individualized*
739 *p.p.b.-range mass accuracies and proteome-wide protein quantification.* Nat Biotechnol,
740 2008. **26**(12): p. 1367-72.
741 78. Adachi, A., et al., *Production of acquired immunodeficiency syndrome-associated retrovirus*
742 *in human and nonhuman cells transfected with an infectious molecular clone.* J Virol, 1986.
743 **59**(2): p. 284-91.
744 79. Rodenburg, C.M., et al., *Near full-length clones and reference sequences for subtype C*
745 *isolates of HIV type 1 from three different continents.* AIDS Res Hum Retroviruses, 2001.
746 **17**(2): p. 161-8.
747 80. Van Heuverswyn, F., et al., *Genetic diversity and phylogeographic clustering of SIVcpzPtt in*
748 *wild chimpanzees in Cameroon.* Virology, 2007. **368**(1): p. 155-71.
749 81. Ahuka-Mundeke, S., et al., *Full-length genome sequence of a simian immunodeficiency virus*
750 *(SIV) infecting a captive agile mangabey (Cercocebus agilis) is closely related to SIVrcm*

751 *infecting wild red-capped mangabeys (Cercocebus torquatus) in Cameroon.* J Gen Virol, 2010.
752 **91**(Pt 12): p. 2959-64.
753 82. Gnanadurai, C.W., et al., *Genetic identity and biological phenotype of a transmitted/founder*
754 *virus representative of nonpathogenic simian immunodeficiency virus infection in African*
755 *green monkeys.* J Virol, 2010. **84**(23): p. 12245-54.
756 83. Lopker, M.J., et al., *Derivation and Characterization of Pathogenic Transmitted/Founder*
757 *Molecular Clones from Simian Immunodeficiency Virus SIVsmE660 and SIVmac251 following*
758 *Mucosal Infection.* J Virol, 2016. **90**(19): p. 8435-53.
759 84. Guyader, M., et al., *Genome organization and transactivation of the human*
760 *immunodeficiency virus type 2.* Nature, 1987. **326**(6114): p. 662-9.
761 85. Aghokeng, A.F., et al., *Full-length sequence analysis of SIVmus in wild populations of*
762 *mustached monkeys (Cercopithecus cephus) from Cameroon provides evidence for two co-*
763 *circulating SIVmus lineages.* Virology, 2007. **360**(2): p. 407-18.
764 86. Beer, B.E., et al., *Characterization of novel simian immunodeficiency viruses from red-capped*
765 *mangabeys from Nigeria (SIVrcmNG409 and -NG411).* J Virol, 2001. **75**(24): p. 12014-27.
766 87. Hu, J., et al., *Characterization and comparison of recombinant simian immunodeficiency virus*
767 *from drill (Mandrillus leucophaeus) and mandrill (Mandrillus sphinx) isolates.* J Virol, 2003.
768 **77**(8): p. 4867-80.

769

770 ## Figure legends

771 **Figure 1. Proteomic analysis of the effect of Vpr in HIV infection.**

772 **A**, Graphical summary of the HIV and ΔVpr HIV infection TMT experiment. Three replicates of
773 uninfected (mock), WT HIV infected and ΔVpr infected cells were prepared and analysed in parallel
774 using TMT labelling. **B,** FACS plots showing the quantification of infection in an example replicate for
775 each of the three conditions. Infected cells lose CD4 expression and become GFP positive. **C,**
776 Scatterplots displaying pairwise comparisons between WT, ΔVpr and mock-infected cells. Each point
777 represents a single protein, with HIV proteins and host proteins of interest highlighted with different
778 symbols (see key). **D,** Principle component analysis of the samples in this experiment, with WT
779 infected replicates in red, ΔVpr in blue and mock infected cells in grey.

780 **Figure 1 – source data 1. Interactive database of protein changes in the datasets presented here.**

781 **Figure 2. Analysis of the nature of Vpr mediated proteome remodelling.**

782 **A**, Graphical summary of the Vpr viral particle TMT experiment. Three replicates of cells exposed to
783 empty viral particles or Vpr bearing viral particles, along with single replicates of cells exposed to
784 viral particles bearing five different Vpr mutants were prepared and analysed in parallel using TMT
785 labelling. **B,** Scatterplot displaying pairwise comparison between cells exposed to empty or Vpr
786 bearing viral particles. **C**, Scatterplot comparing pairwise comparisons from two proteomics
787 experiments, demonstrating the effect of Vpr in the context of HIV-1 infection (x-axis, as shown in
788 **Figure 1A**) or through cellular exposure to Vpr protein alone (y- axis, as shown in **Figure 2A**). **D**,
789 scatterplots showing the pairwise comparison between each Vpr mutant tested and empty vector
790 control, with defined groups of 302 Vpr depleted and 413 increased proteins highlighted in blue and
791 red respectively. **E**, Heatmap showing the behaviour of the 100 proteins most depleted by Vpr
792 particles (blue) and increased (red) within the defined highly modulated subsets. Colour indicates
793 the $\log_2$ fold change of each protein in each condition compared to empty particle treatment. Genes

794 were clustered using uncentered Pearson correlation and centroid linkage, and conditions clustered
795 by column means.

796 **Figure 2 – figure supplement 1. Example proteins modulated by Vpr**

797 **A,** Scatterplots displaying pairwise comparisons between WT, ΔVpr and mock-infected cells. Vpr
798 depleted proteins confirmed by blot in this figure are highlighted in blue, UNG, ZGPAT and HLTF are
799 previously identified targets for Vpr mediated degradation, shown in purple. CCNB1 is increased by
800 Vpr (red). **B,** Scatterplot displaying pairwise comparison between cells exposed to empty or Vpr
801 bearing viral particles. **C,** Scatterplot comparing pairwise comparisons from two proteomics
802 experiments, demonstrating the effect of Vpr in the context of HIV-1 infection (as shown in **Figure**
803 **1A**, x-axis) or through cellular exposure to Vpr protein alone (**Figure 2A**, y-axis). **D,** Bar charts
804 showing the Vpr mediated changes in protein abundance in both proteomics experiments of the
805 proteins highlighted in this figure. **e,** Immunoblot of proteins highlighted in this figure.

806 **Figure 2 – figure supplement 2. Additional details of the Vpr WT and Mutant experiment in Figure**
807 **2.**

808 **A,** Immunoblot of purified virus preparations used to infect cells for the proteomics experiment
809 displayed in **Fig 2A**. **B,** Bar chart showing the average scaled abundance of matrix, capsid and
810 integrase peptides detected in the cell lysate by MS. Bars show mean and standard deviation. **c,** 7-
811 AAD stain of cells exposed to empty vector, or Vpr wild type or Vpr mutants. Watson pragmatic
812 modelling was used to identify cells in G1 (blue), S (grey) or G2/M (red) phase.

813 **Figure 2 - figure supplement 3. Quantifying the effect of Vpr under reduced DCAF1 conditions.**

814 **A,** Graphical summary of the DCAF1 KD experiment. **B,** Scatterplot displaying pairwise comparison
815 between Sh-Control and Sh-DCAF1 cells at 0 h, with defined groups of 302 Vpr depleted (blue) and
816 413 increased (red) proteins highlighted. DCAF1 is highlighted in purple. **C,** Example time-course
817 behaviour for one Vpr target (HLTF) and one secondary Vpr effect (CCNB1). **D,** Scatterplots showing
818 the pairwise comparison between the 6 or 24 h timepoint with the 0 h condition for each sh-
819 transduced cell line.

820 **Figure 2- figure supplement 4. Cell cycle regulation of Vpr modulated proteins.**

821 **A,** Ly, 2015 contains a proteomic analysis of NB4 cells treated with RO-3306 cells arrested in G2/M
822 with the PLK1 inhibtor RO-3306. Scatterplot showing the pairwise comparison of abundance of
823 proteins isolated from RO-3306 treated vs mock treated cells. Groups of proteins defined in the
824 current study of 302 Vpr depleted (blue) and 413 increased (red) proteins are highlighted, indicating
825 the behaviour of these proteins in NB4 cells arrested at G2/M.

826 **B,** Correlation of the Vpr mediated change in cyclin abundance in the present study (x-axis), with RO-
827 3306 mediated changes in NB4 cells in Ly, 2015. Changes in cyclin abundance in HIV infection are
828 assumed to be secondary to cell cycle arrest, and thus this correlation indicates the concordance
829 between effects secondary to cell cycle arrest between the two datasets.

830 **C,** Pie charts showing the overlap between changes in the present study and changes induced by
831 G2/M arrest in Ly, 2015. Left panel shows the behaviour of all proteins quantified in both the
832 present study (**Figure 1A** and **Figure 2A**) and Ly, 2015, i.e. a total of 1643 proteins were quantified in
833 both datasets, of which 1100 proteins did not significantly change in G2/M arrest, 260 proteins were
834 significantly depleted in G2/M arrested cells, and 283 proteins were significantly increased in G2/M

835 arrested cells. Middle panel shows the behaviour the defined group of 302 Vpr depleted proteins.
836 I.e. of 302 proteins, a total of 90 proteins were detected in Ly, 2015, 58 of which did not significantly
837 change in G2/M arrest, 18 were significantly depleted in G2/M arrest and 14 were significantly
838 increased in G2/M arrest. † Indicates the fraction in each case where the change induced by cell
839 cycle arrest is in the same direction as the effect of Vpr, i.e. the fraction for which cell cycle arrest
840 could explain the Vpr mediated protein changes. Right panel shows the behaviour of the defined
841 group of 413 Vpr increased proteins.

842 **D,** Fischer, 2016, define lists of 115 proteins whose expression peaks in G1/S phase and 174 proteins
843 whose expression peaks in G2/M phase. Pie-charts show the overlap between these lists and (left)
844 all proteins detected in the present study, (middle) proteins defined as being depleted by Vpr, and
845 (right) proteins defined as being increased by Vpr. As in the proteomics dataset, there is some
846 enrichment of proteins with peak expression in G2/M within Vpr increased proteins, and some
847 enrichment of proteins with peak expression in G1/S in Vpr depleted proteins, consistent with some
848 effects being secondary to cell cycle arrest, but these effects are in the minority.

849 **Figure 2 – figure supplement 5. Role of MCM10 in Vpr medated G2/M arrest.**

850 **A,** Correlation between depletion of MCM10 by each Vpr mutant tested and the extent of G2/M
851 arrest caused by that mutant, red line shows linear regression analysis. **B,** Example DNA staining
852 showing G2/M arrest caused by shRNA mediated depletion of MCM10, representative of three
853 independent experiments. Watson pragmatic modelling was used to identify cells in G1 (blue), S
854 (grey) or G2/M (red) phase. **C**, Real-time qRT-PCR analysis of MCM10 mRNA abundance in cells
855 transduced with control or MCM10 targeting shRNA. Values were generated using the ΔΔCT
856 method, relative to GAPDH mRNA abundance and normalised to the control condition. Bars show
857 mean values, error bars show SEM of three technical replicates.

858 **Figure 3. Gene ontology enrichment analysis for proteins depleted or increased by Vpr**

859 Defined groups of Vpr depleted and increased proteins were subject to gene ontology enrichment
860 analysis, compared with a background of all proteins quantitated in these experiments. **A,** Cellular
861 compartment analysis – GO enrichment analysis results were manually curated for 9 commonly used
862 organelle level classifications, shown here. + / - indicates if the classification was enriched or de-
863 enriched compared with the expected number of proteins expected by chance. Where significant,
864 associated p value represents the results of a Fisher's exact test with Bonferroni correction. This is
865 highly conservative as it is corrected for all 1061 possible cellular compartment terms, not just those
866 shown. **B,** Molecular function analysis. Plots show all significantly enriched (Fisher's exact test with
867 Bonferroni correction) molecular function terms with associated p values. In all cases, proteins with
868 no available compartment or function classification were removed from the denominator.

869 **Figure 4. MS-IP approach to identify direct targets for Vpr mediated degradation.**

870 **A,** Graphical summary of the MS-IP experiment. All cells were stably transduced with an ShDCAF1
871 vector as described earlier. MLN4924 is a pan-Cullin inhibitor. **B,** 20 most abundant proteins
872 identified by Co-IP determined by number of unique peptides, normalised as a proportion of the
873 maximum possible peptide count for each protein, (Exponentially modified protein abundance
874 index, emPAI). Proteins falling within the defined list of 302 Vpr depleted and 413 Vpr increased
875 proteins are highlighted in blue and red respectively. **C,** The same 20 proteins with signal intensity
876 rather than peptide number shown. **D,** Pie chart indicating the overlap between the proteins co-
877 immunoprecipitated with Vpr and the defined list of 302 Vpr decreased (blue) and 413 Vpr increased

878 proteins (red), and proteins detected but falling into neither list (grey). **E**, Bar chart showing the
879 enrichment of Vpr depleted and Vpr increased proteins within proteins co-immunoprecipitated with
880 Vpr compared to the expected numbers of proteins that would be co-immunopreciptated from each
881 group by chance. p-value indicates a Fisher's exact test of a 2x2 contingency table (Vpr
882 depleted/increased, identified by co-IP/not identified), indicating that the two criteria are
883 significantly linked.

884 **Figure 5. Pulsed SILAC method to identify direct targets for Vpr mediated decay.**

885 **A,** Graphical summary of the pulsed SILAC experiment. **B,** Scatterplots showing the changes to
886 protein stability of proteins after 6 or 24 hours of exposure to Vpr bearing lentivirus compared to
887 control lentivirus, with defined groups of 302 Vpr depleted (blue) and 413 increased (red) proteins
888 highlighted. **C,** Expanded view of proteins degraded within 6 hours of Vpr exposure. Significantly
889 degraded (Sig.B <0.01) proteins are highlighted in gold. Previously described Vpr targets HLTF,
890 MUS81 and ZGPAT are shown in purple.

891 **Table 1. Direct targets for Vpr mediated degradation**

892 Summary of the direct targets for Vpr mediated degradation. Proteins highlighted in purple are
893 previously described Vpr targets, proteins with red text were predicted as potential Vpr targets
894 based on their temporal profile of depletion in Greenwood & Matheson, 2016 [5].

895 **Table 1 – table supplement 1. Behaviour of previously identified direct Vpr targets.**

896 **Figure 6. Novel Vpr targets involved in G2/M arrest.**

897 **A,** Targeted shRNA screen of direct Vpr target proteins identified here, whose depletion correlated
898 with G2/M arrest in **Figure 2.** Bars show averages of at least two replicates from more than three
899 independent experiments, error bars showing SEM. Lines show control average +/- 3 standard
900 deviations. Control condition contains combined data from three different control shRNA. **B,** Real-
901 time qRT-PCR analysis of mRNA abundance in cells transduced with control or targeting shRNA.
902 Values were generated using the ΔΔCT method, relative to GAPDH mRNA abundance and normalised
903 to the control condition. Bars show mean values, error bars show SEM of three technical replicates.
904 **C,** Example DNA staining showing G2/M arrest caused by shRNA mediated depletion of SMN1,
905 CDCA2 and ZNF267, representative of at least two independent experiments.

906 **Figure 7. Identification of proteome changes conserved between human and primate lentiviral Vpr**
907 **lineages. A**, Graphical summary of the TMT experiment testing conservation of Vpr functions. **b**,
908 Scatterplots showing the pairwise comparison between each Vpr tested and empty vector control
909 with defined groups of 302 Vpr depleted (blue) and 413 increased (red) proteins highlighted. **C,**
910 Heatmap showing the behaviour of the 100 proteins most depleted by Vpr particles (blue) and
911 increased (red) within the defined highly modulated subsets. Colour indicates the $\log_2$ fold change of
912 each protein in each condition compared to empty vector virus transduction. **D,** Bar chart showing
913 the significantly Vpr depleted group showing profound (more than 50%) depletion in more than one
914 lineage, of the four lineages tested (HIV-1/SIVcpz, HIV-2/SIVsmm, SIVagm, SIVrcm). Gold bars
915 indicate proteins identified as direct targets for Vpr mediated degradation, DCAF1, known to interact
916 with multiple lineages, is highlight in purple. **E**, Immunoblot of example known, non-conserved and
917 conserved targets of Vpr mediated depletion. N.B. The HIV-2 Vpr is a primary isolate HIV-2 Vpr
918 (7312a), while the proteomics experiment included HIV-2 ROD Vpr.

919 **Figure 7 – figure supplement 1. Additional information relating to expanded panel of primate**
920 **lentiviral Vpr and Vpx varients.**

921 **A,** %GFP positive (transduced) cells at harvest. Cells were transduced at an infectious MOI of 1.5
922 based on prior titration, with the actual resulting % transduction varying slightly across the samples.
923 **B**, Proportion of cells in G2/M at point of harvest based on 7-AAD staining and Watson pragmatic
924 modelling. **B,** Scatterplots displaying pairwise comparisons between Vpr/Vpx transduced cells and
925 empty vector. Labelled proteins are direct targets for Vpr mediated degradation that are depleted by
926 Vpr varients from at least 3 different lineages.

927 **Figure 8. Depletion of HuSH components by lentiviral Vpx and Vpr proteins.**

928 **A,** Scatterplots showing the pairwise comparison between each Vpr tested and empty vector control
929 with HuSH complex components highlighted. **B**, Bar graph of GFP percentage positive of JLAT-A1
930 cells after transduction with control (Cre recombinase), Vpr or Vpx proteins and treatment with
931 TNFα. Mean and SEM of 3 biological replicates per condition are shown, representative of three
932 independent similar experiments. p-values determined by ordinary one-way ANOVA with Bonferroni
933 comparison between Vpr/Vpx treatment and control treated cells. **C,** Phylogenetic tree of primate
934 lentiviruses based on an alignment of Vif nucleic acid sequences, with 5 major lineages of primate
935 lentiviruses labelled. Information on Vpr and Vpx activity based on a selected number of isolates
936 tested in each lineage in Lim, 2012 [44] **D,** Immunoblot of TASOR in cells transduced with a panel of
937 Vpx and Vpr proteins.

938 **Figure 9. Extended time-course analysis of HIV-2 primary isolate Vpr and Vpx proteins.**

939 **A**, Graphical summary of the TMT experiment. **B,** Scatterplots displaying pairwise comparison
940 between cells transduced with 7312a HIV-2 Vpr and Vpx for 96 h compared with those transduced
941 with empty vector for 96 h. Blue and red dots represent the defined groups or proteins depleted or
942 increased by NL4-3 Vpr respectively. Points ringed in gold indicate direct targets for NL4-3 Vpr
943 mediated degradation listed in Table 1.

Table 2. Vpr and Vpx variants tested.

Figure 1

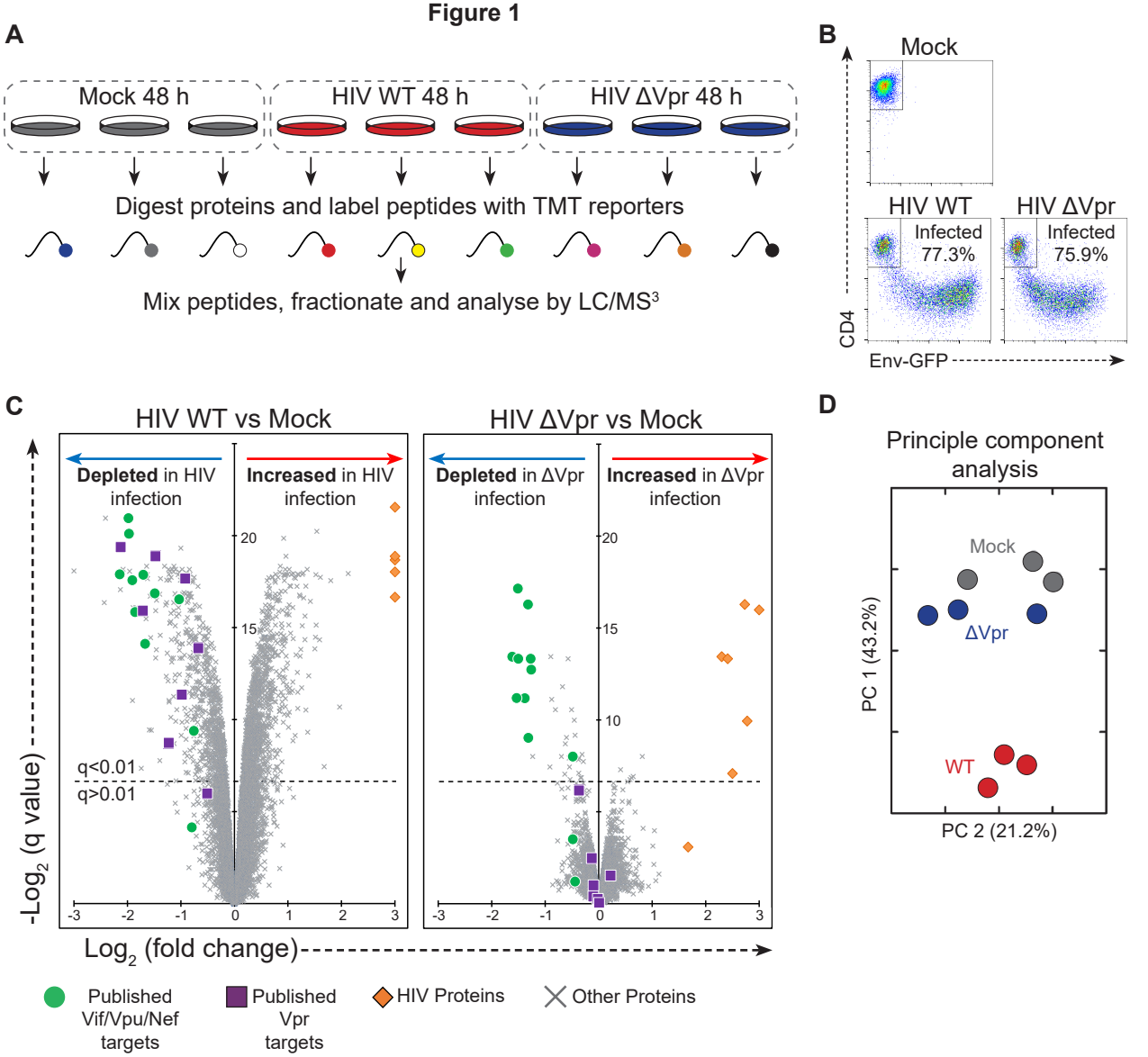
A
Mock 48 h
HIV WT 48 h
HIV ΔVpr 48 h
Digest proteins and label peptides with TMT reporters
Mix peptides, fractionate and analyse by LC/MS3
B
Mock
HIV WT
HIV ΔVpr
Infected 77.3%
Infected 75.9%
CD4
Env-GFP
C
HIV WT vs Mock
HIV ΔVpr vs Mock
Depleted in HIV infection
Increased in HIV infection
Depleted in ΔVpr infection
Increased in ΔVpr infection
q<0.01
q>0.01
-Log2 (q value)
Log2 (fold change)
Published Vif/Vpu/Nef targets
Published Vpr targets
HIV Proteins
Other Proteins
D
Principle component analysis
Mock
ΔVpr
WT
PC 1 (43.2%)
PC 2 (21.2%)

Figure 2

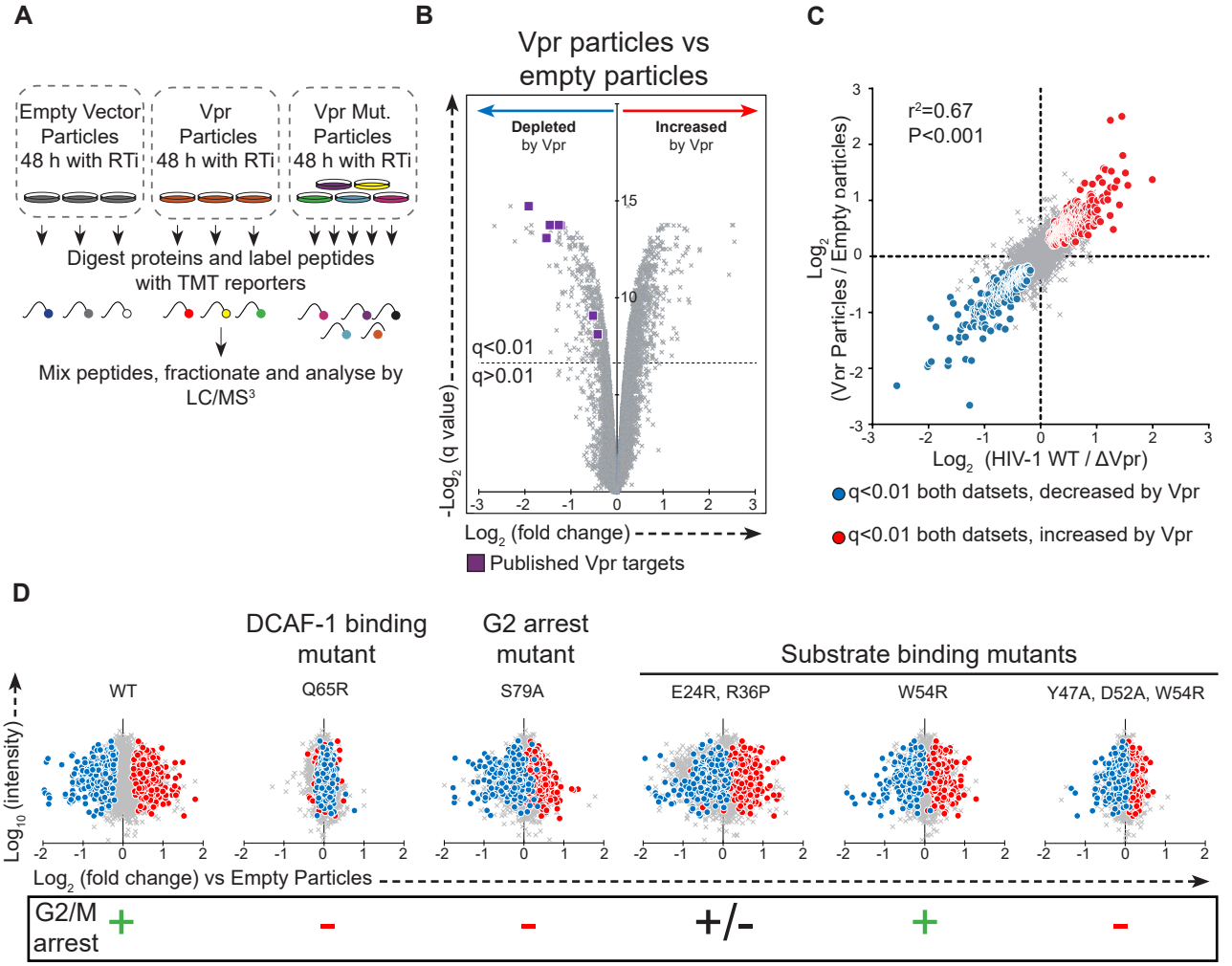
A
Empty Vector Particles 48 h with RTi
Vpr Particles 48 h with RTi
Vpr Mut. Particles 48 h with RTi
Digest proteins and label peptides with TMT reporters
Mix peptides, fractionate and analyse by LC/MS³
B
Vpr particles vs empty particles
Depleted by Vpr
Increased by Vpr
q<0.01
q>0.01
-Log2 (q value)
Log2 (fold change)
Published Vpr targets
C
r²=0.67
P<0.001
Log2 (Vpr Particles / Empty particles)
Log2 (HIV-1 WT / ΔVpr)
q<0.01 both datsets, decreased by Vpr
q<0.01 both datsets, increased by Vpr
D
DCAF-1 binding mutant
G2 arrest mutant
Substrate binding mutants
WT
Q65R
S79A
E24R, R36P
W54R
Y47A, D52A, W54R
Log10 (intensity)
Log2 (fold change) vs Empty Particles
G2/M arrest
+
-
-
+/-
+
-

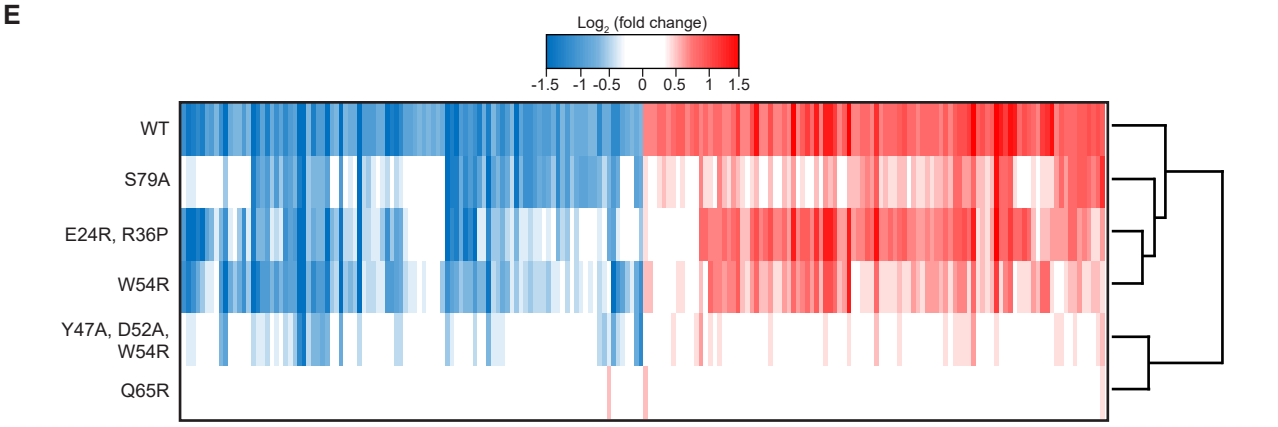
E
Log2 (fold change)
-1.5 -1 -0.5 0 0.5 1 1.5
WT
S79A
E24R, R36P
W54R
Y47A, D52A, W54R
Q65R

Figure 2 - figure supplement 1

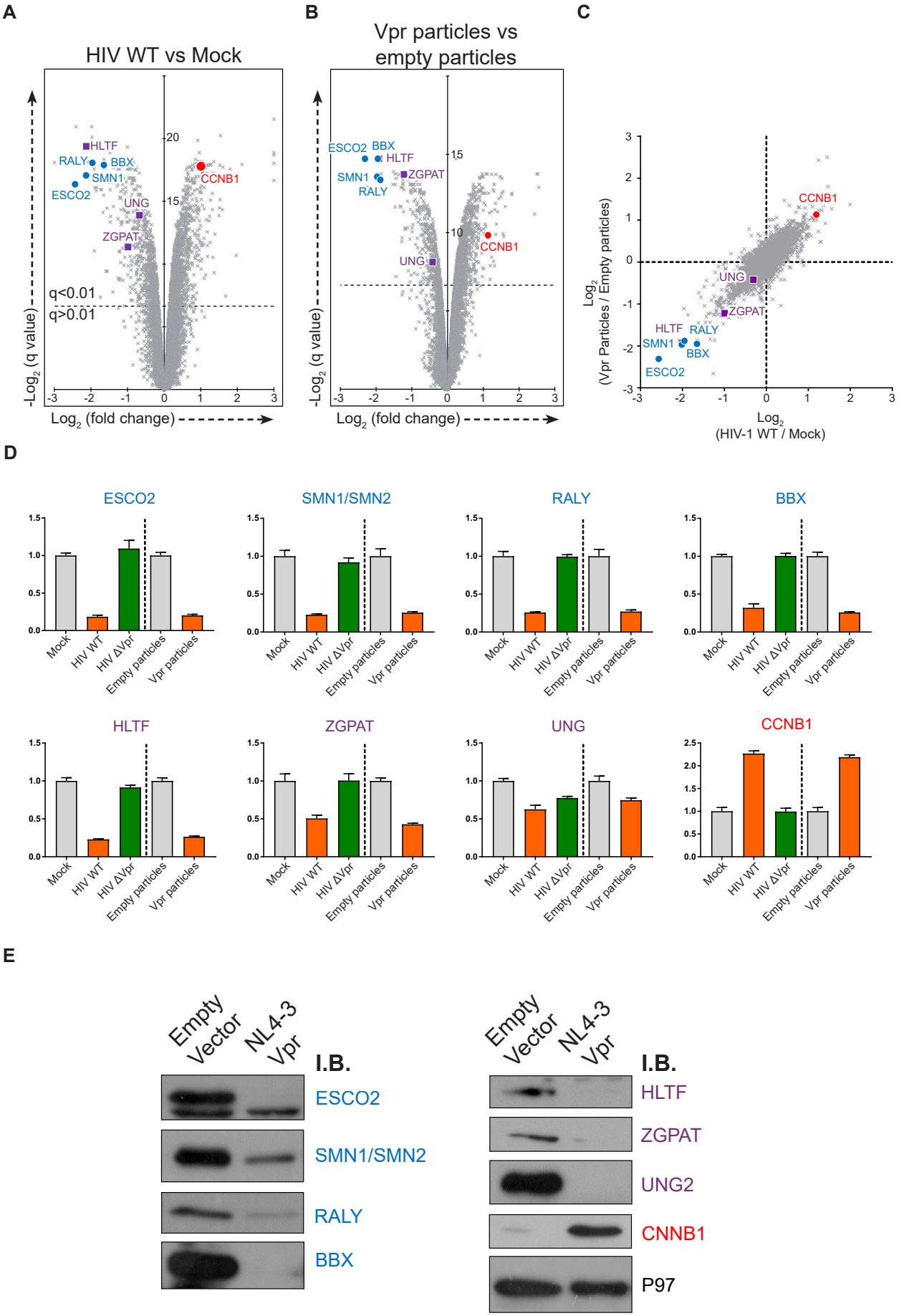

Figure 2 - figure supplement 2

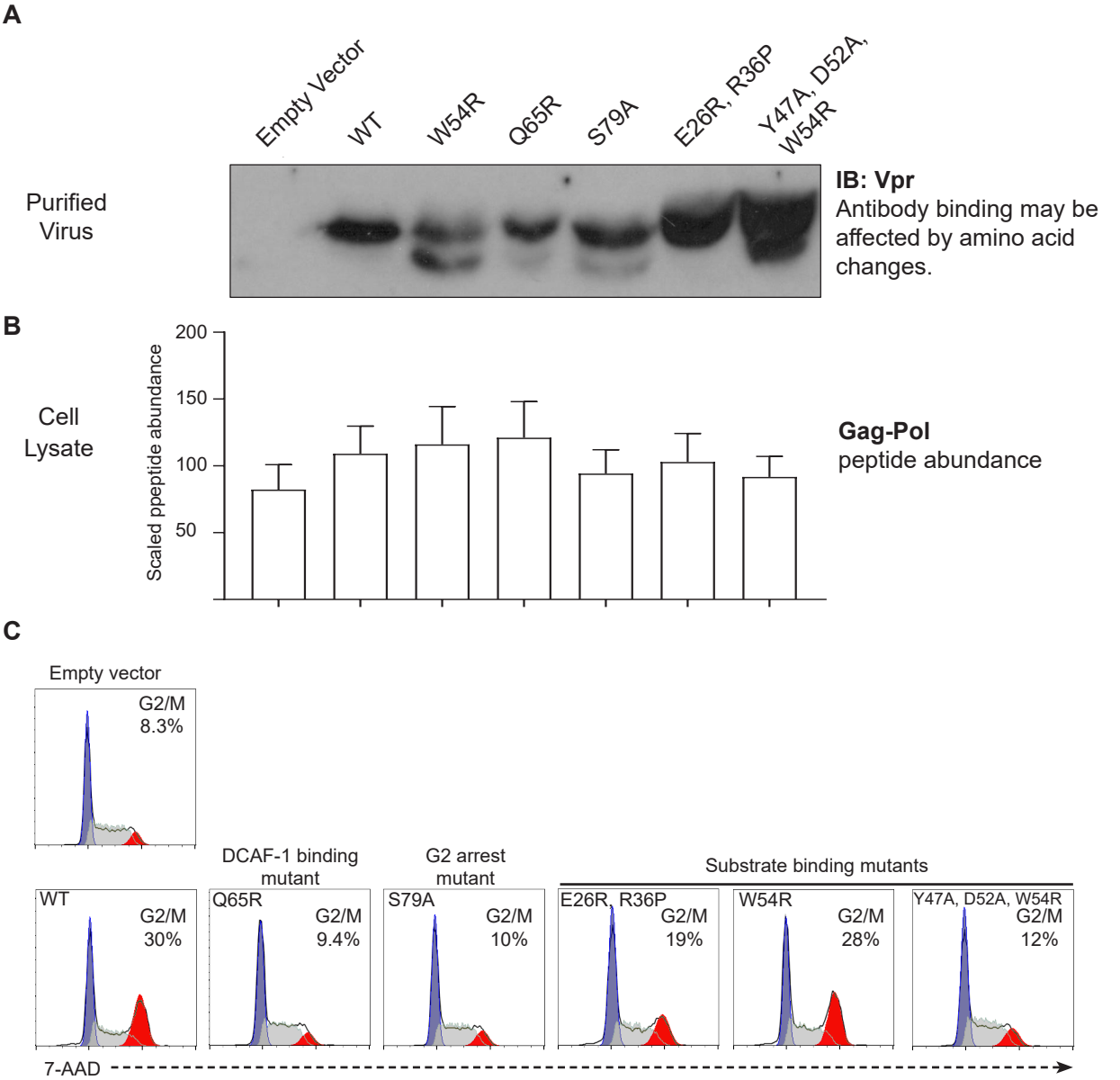

Figure 2 - figure supplement 3

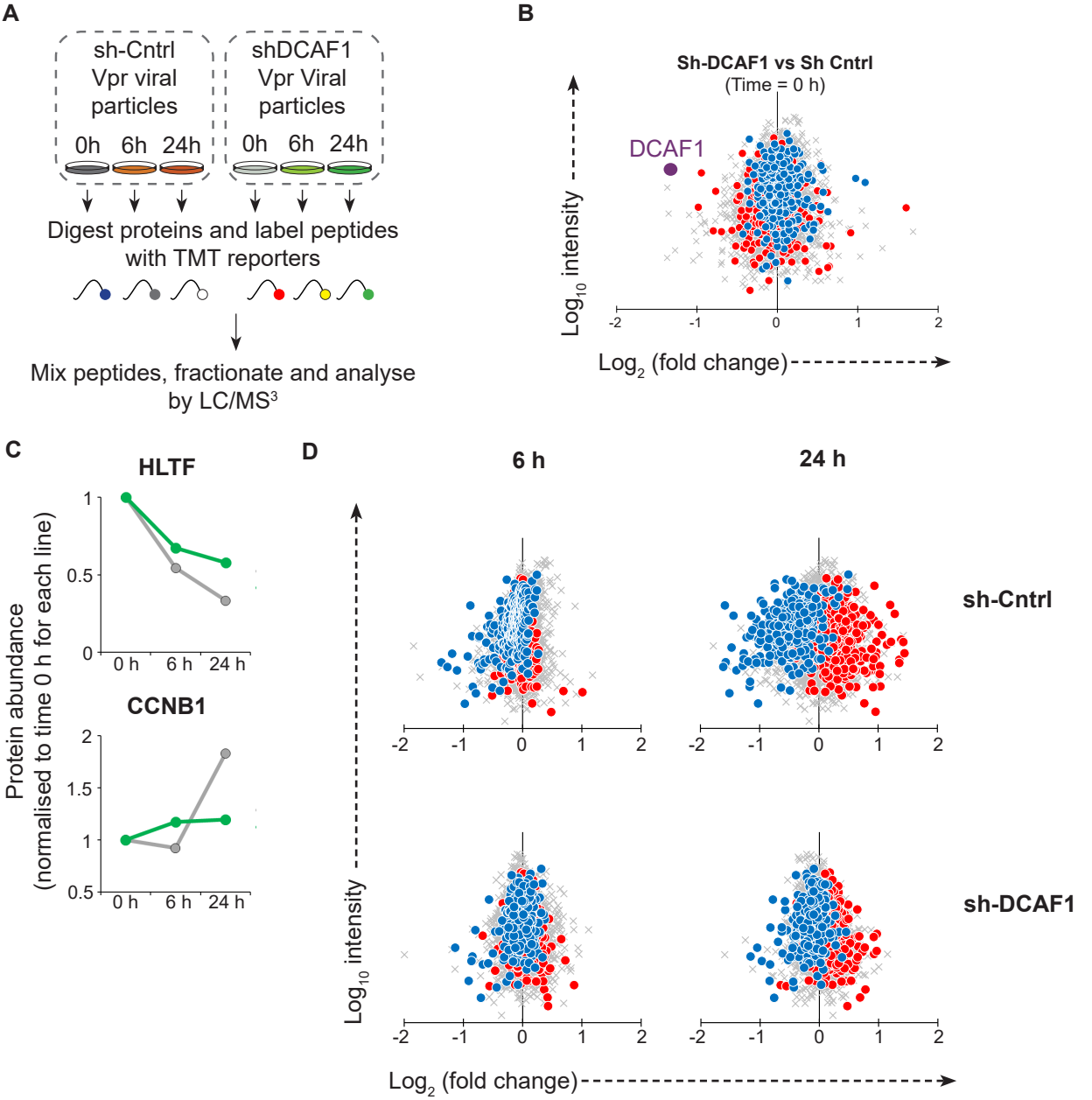

Figure 2 - figure supplement 4

A Ly, 2015, Proteomics in cells arrested at G2/M using PLK1 inhibitor RO-3306

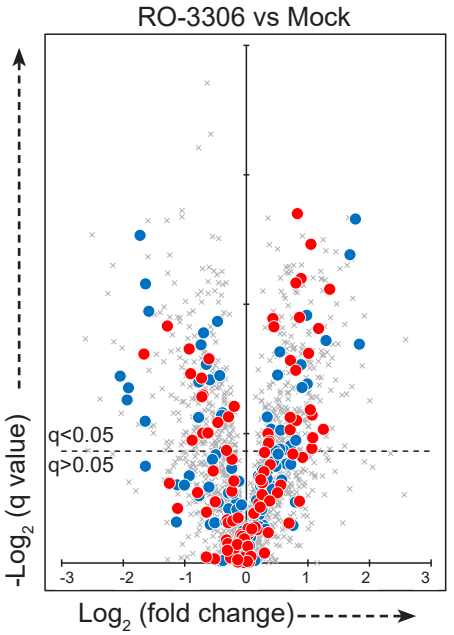

B

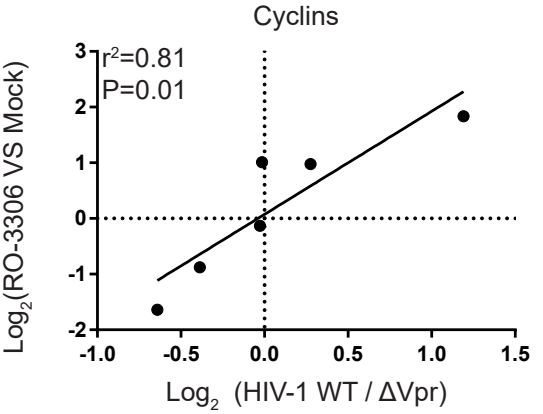

C

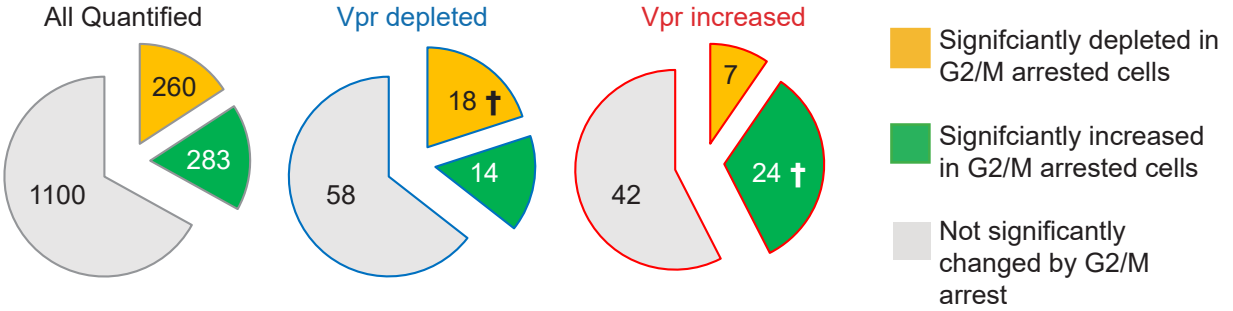

D Fischer, 2016 - Transcriptional anlalysis

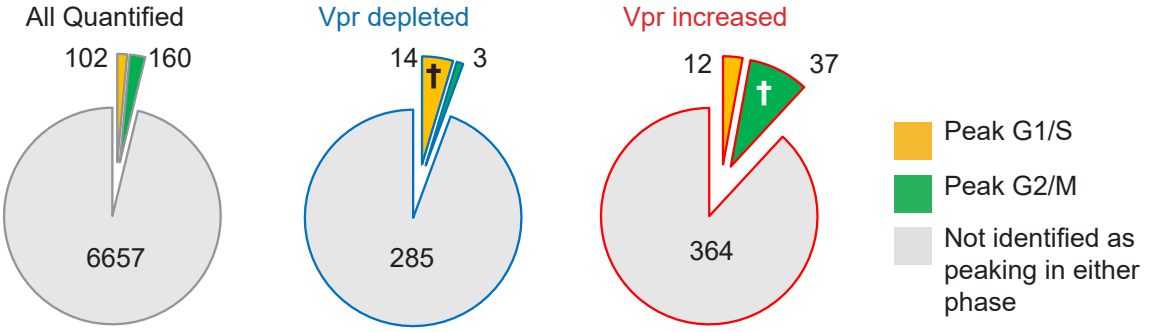

Figure 2 - figure supplement 5

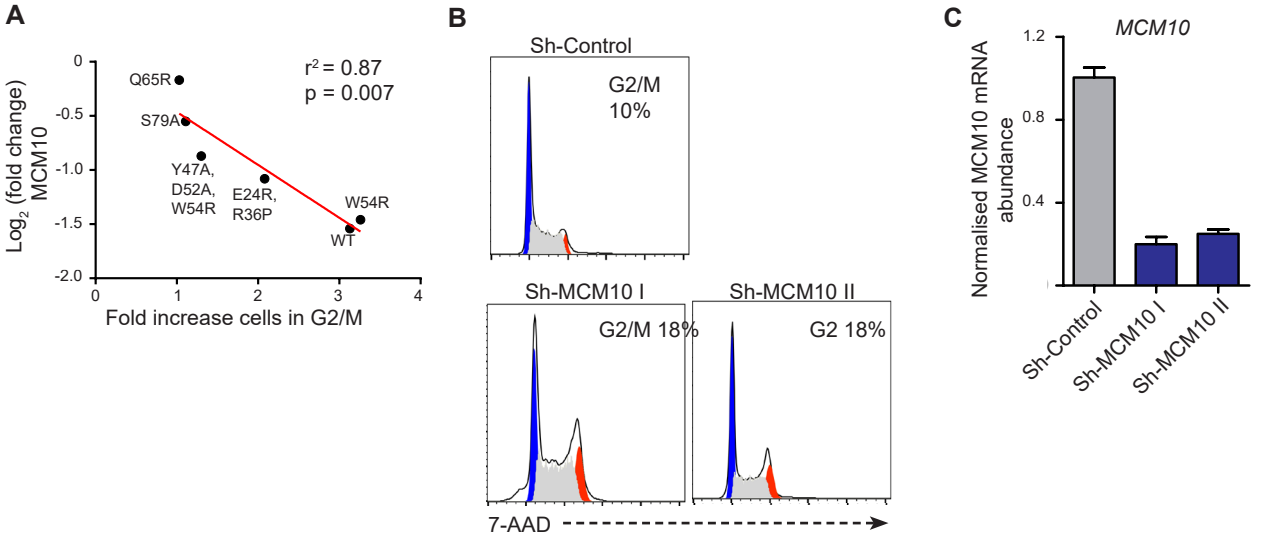

Figure 3

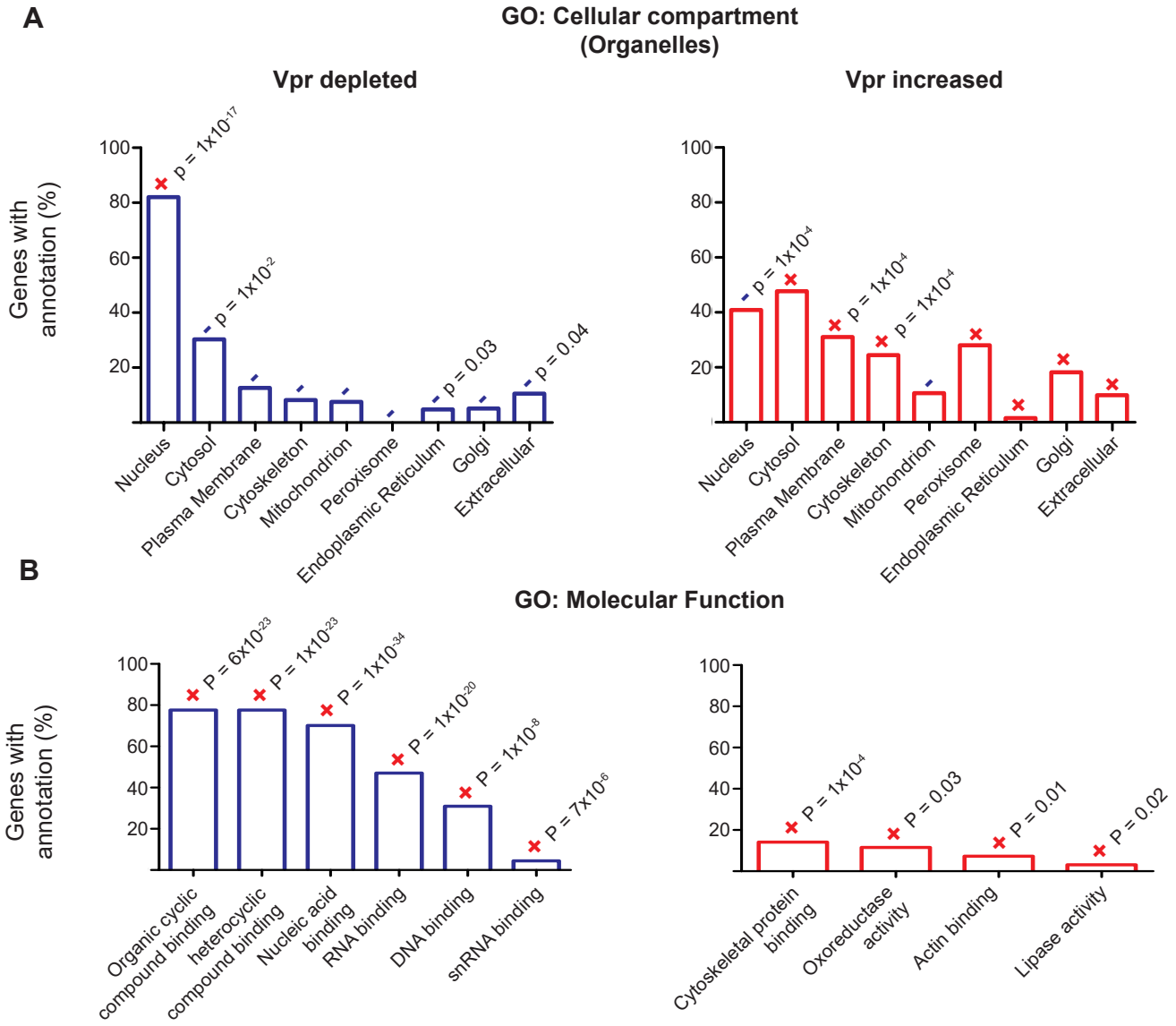
A
GO: Cellular compartment
(Organelles)
Vpr depleted
Vpr increased
Genes with annotation (%)
100
80
60
40
20
p = 1x10-17
p = 1x10-2
p = 0.03
p = 0.04
p = 1x10-4
p = 1x10-4
p = 1x10-4
Nucleus
Cytosol
Plasma Membrane
Cytoskeleton
Mitochondrion
Peroxisome
Endoplasmic Reticulum
Golgi
Extracellular
B
GO: Molecular Function
P = 6x10-23
P = 1x10-23
P = 1x10-34
P = 1x10-20
P = 1x10-8
P = 7x10-6
P = 1x10-4
P = 0.03
P = 0.01
P = 0.02
Organic cyclic compound binding
heterocyclic compound binding
Nucleic acid binding
RNA binding
DNA binding
snRNA binding
Cytoskeletal protein binding
Oxoreductase activity
Actin binding
Lipase activity

Figure 4

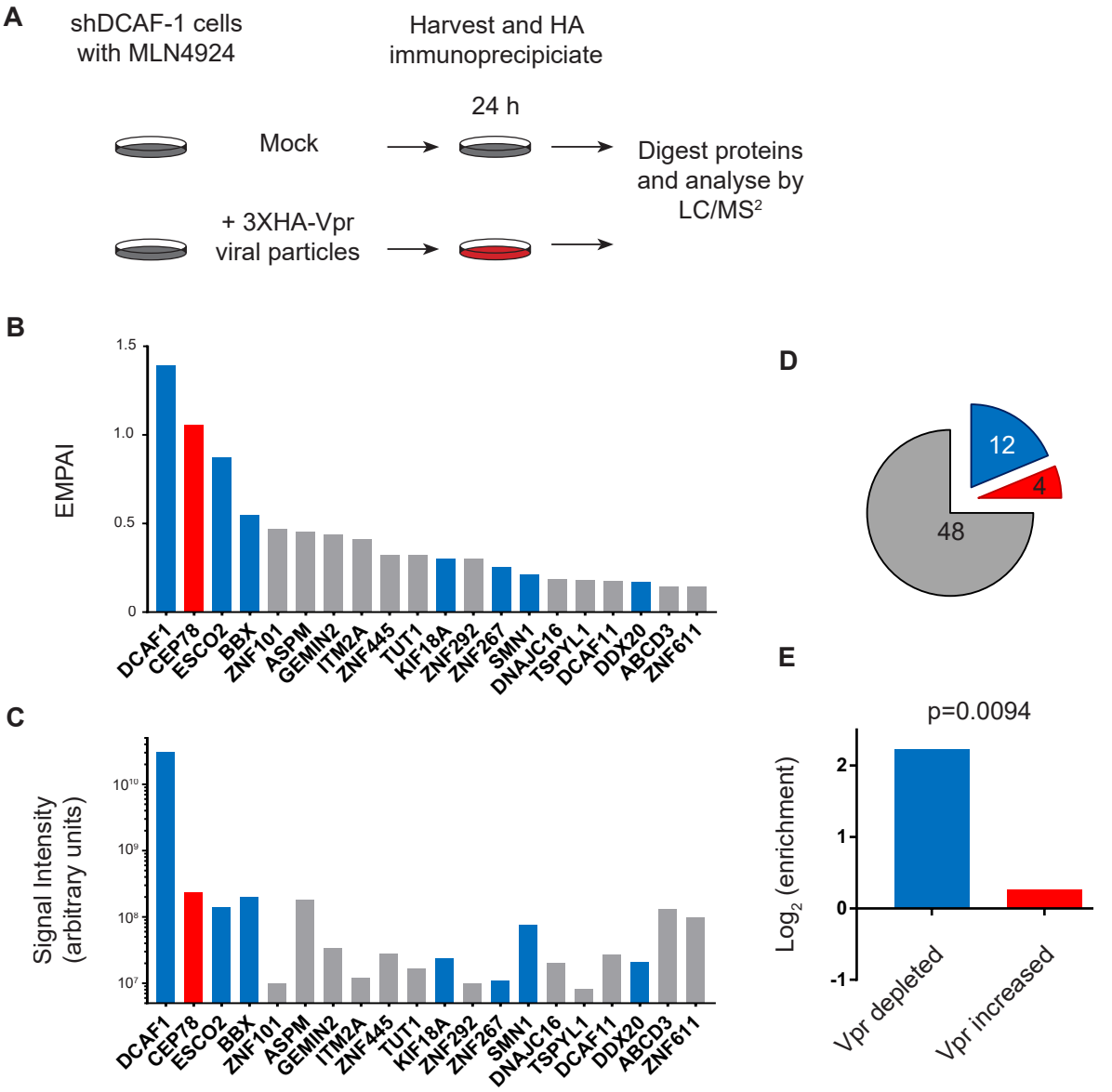
A
shDCAF-1 cells with MLN4924
Harvest and HA immunoprecipiciate
24 h
Mock
+ 3XHA-Vpr viral particles
Digest proteins and analyse by LC/MS²
B
EMPAI
1.5
1.0
0.5
0
DCAF1
CEP78
ESCO2
BBX
ZNF101
ASPM
GEMIN2
ITM2A
ZNF445
TUT1
KIF18A
ZNF292
ZNF267
SMN1
DNAJC16
TSPYL1
DCAF11
DDX20
ABCD3
ZNF611
C
Signal Intensity (arbitrary units)
10¹⁰
10⁹
10⁸
10⁷
DCAF1
CEP78
ESCO2
BBX
ZNF101
ASPM
GEMIN2
ITM2A
ZNF445
TUT1
KIF18A
ZNF292
ZNF267
SMN1
DNAJC16
TSPYL1
DCAF11
DDX20
ABCD3
ZNF611
D
12
4
48
E
p=0.0094
Log₂ (enrichment)
2
1
0
-1
Vpr depleted
Vpr increased

Figure 5

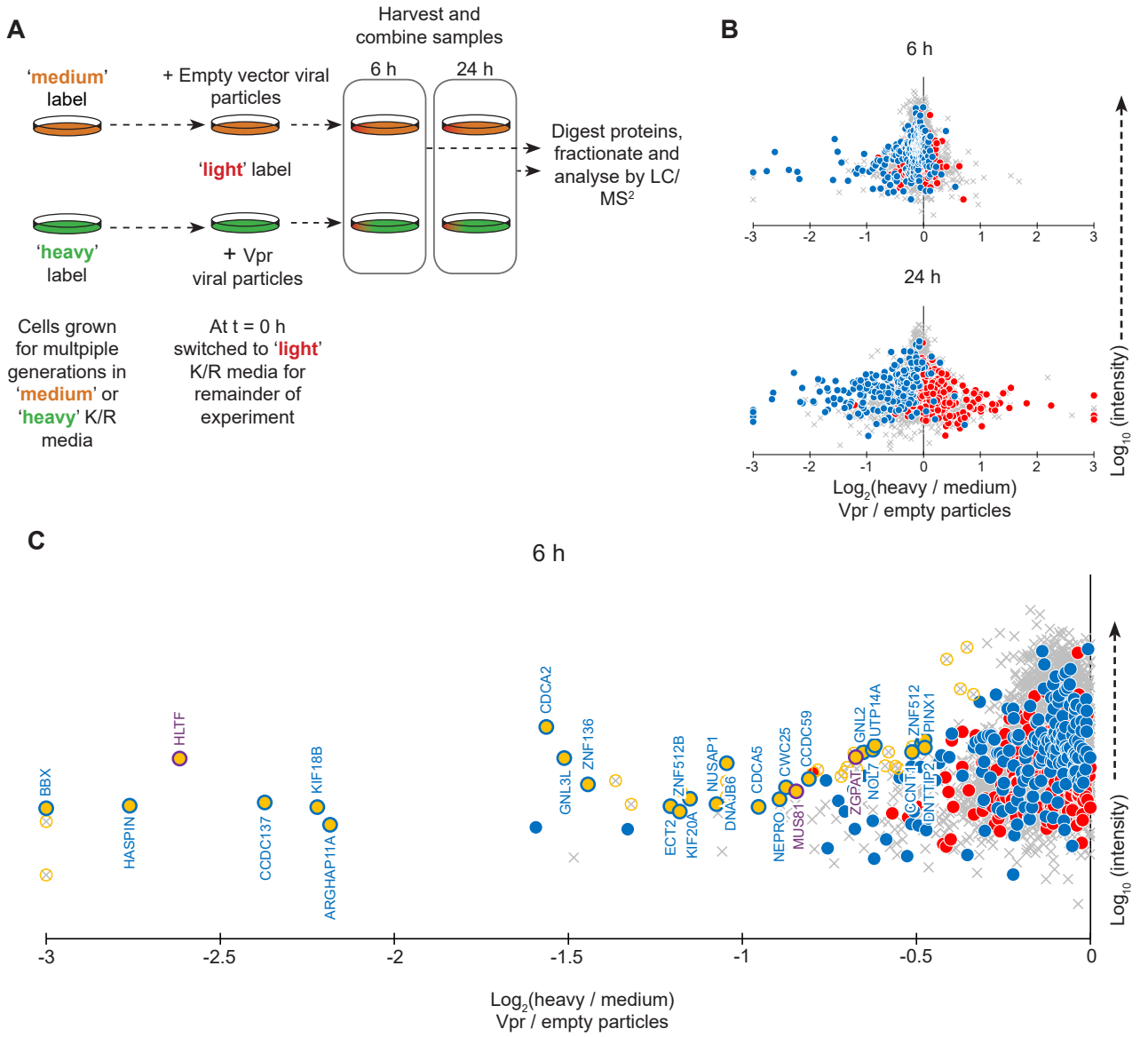
A
Harvest and combine samples
'medium' label
+ Empty vector viral particles
6 h
24 h
'light' label
Digest proteins, fractionate and analyse by LC/MS²
'heavy' label
+ Vpr viral particles
Cells grown for multpiple generations in 'medium' or 'heavy' K/R media
At t = 0 h switched to 'light' K/R media for remainder of experiment
B
6 h
24 h
Log₁₀ (intensity)
Log₂(heavy / medium)
Vpr / empty particles
C
6 h
BBX
HASPIN
HLTF
CCDC137
KIF18B
ARGHAP11A
CDCA2
GNL3L
ZNF136
ECT2
ZNF512B
KIF20A
NUSAP1
DNAJB6
CDCA5
NEPRO
CWC25
MUS81
CCDC59
ZGPAT
GNL2
NOL7
UTP14A
CCNT1
ZNF512
DNTTIP2
PINX1
-3
-2.5
-2
-1.5
-1
-0.5
0
Log₂(heavy / medium)
Vpr / empty particles
Log₁₀ (intensity)

Table 1

Accession	Gene	Vpr necessary	Incoming Vpr sufficient	Degraded within 6 h	Co-IP
Q56NI9	ESCO2	Yes	Yes	ND	Yes
Q16637	SMN1 / SMN2	Yes	Yes	NS	Yes
Q14527	HLTF	Yes	Yes	Yes	-
Q96KM6	ZNF512B	Yes	Yes	Yes	-
Q8WY36	BBX	Yes	Yes	Yes	Yes
A6NFI3	ZNF316	Yes	Yes	Yes	-
Q8NI77	KIF18A	Yes	Yes	ND	Yes
Q8TF76	HASPIN	Yes	Yes	Yes	-
Q9Y4B6	VPRBP	Yes	Yes	NS	Yes
Q96FF9	CDCA5	Yes	Yes	Yes	-
Q6PK04	CCDC137	Yes	Yes	Yes	-
Q9NXE8	CWC25	Yes	Yes	Yes	-
Q86Y91	KIF18B	Yes	Yes	Yes	-
Q6P4F7	ARHGAP11A	Yes	Yes	Yes	-
Q6NW34	NEPRO	Yes	Yes	Yes	-
Q9BVJ6	UTP14A	Yes	Yes	Yes	-
Q9NVN8	GNL3L	Yes	Yes	Yes	-
Q5QJE6	DNTTIP2	Yes	Yes	Yes	-
Q69YH5	CDCA2	Yes	Yes	Yes	-

Accession	Gene	Vpr necessary	Incoming Vpr sufficient	Degraded within 6 h	Co-IP
Q96BK5	PINX1	Yes	Yes	Yes	-
Q8N5A5	ZGPAT	Yes	Yes	Yes	-
Q13823	GNL2	Yes	Yes	Yes	-
Q9UHI6	DDX20	Yes	Yes	NS	Yes
Q96ME7	ZNF512	Yes	Yes	Yes	-
Q14586	ZNF267	Yes	Yes	NS	Yes
Q9H8V3	ECT2	Yes	Yes	Yes	-
P57678	GEMIN4	Yes	Yes	NS	Yes
P52701	MSH6	Yes	Yes	NS	Yes
O75190	DNAJB6	Yes	Yes	Yes	-
Q96NY9	MUS81	Yes	Yes	Yes	-
O60563	CCNT1	Yes	Yes	Yes	-
Q9P031	CCDC59	Yes	Yes	Yes	-
Q9UIS9	MBD1	Yes	Yes	NS	Yes
Q9UMY1	NOL7	Yes	Yes	Yes	-
Q6ZN55	ZNF574	Yes	Yes	NS	Yes
Q9BXS6	NUSAP1	Yes	Yes	Yes	-
O95235	KIF20A	Yes	Yes	Yes	-
P35251	RFC1	Yes	Yes	NS	Yes

ND: Not detected in this experiment
NS: Degraded with Sig.B >0.01

Table 1 - Supplement 1

Accession	Gene	Vpr necessary	Incoming Vpr sufficient	Degraded within 6 h	Co-IP	In direct target list (Fig. 3d)?
Q14527	HLTF	Yes	Yes	Yes	-	Yes
Q7L590	MCM10	Yes	Yes	ND	-	No - Not detected in 6 hour pulsed SILAC or IP
Q8N5A5	ZGPAT	Yes	Yes	Yes	-	Yes
Q96AY2	EME1	Yes	Yes	NS	-	No - depleted but with a Sig.B value of >0.01 in the pulsed SILAC experiment, not detected in IP
Q96NY9	MUS81	Yes	Yes	Yes	-	Yes
Q6N021	TET2	Yes	ND	ND	-	No - Not detected in incoming Vpr experiment (Fig. 2a)
P13051	UNG	Yes	Yes	NS	-	No - depleted but with a Sig.B value of >0.01 in the pulsed SILAC experiment. Detected in the Co-IP but with a single peptide

Figure 6

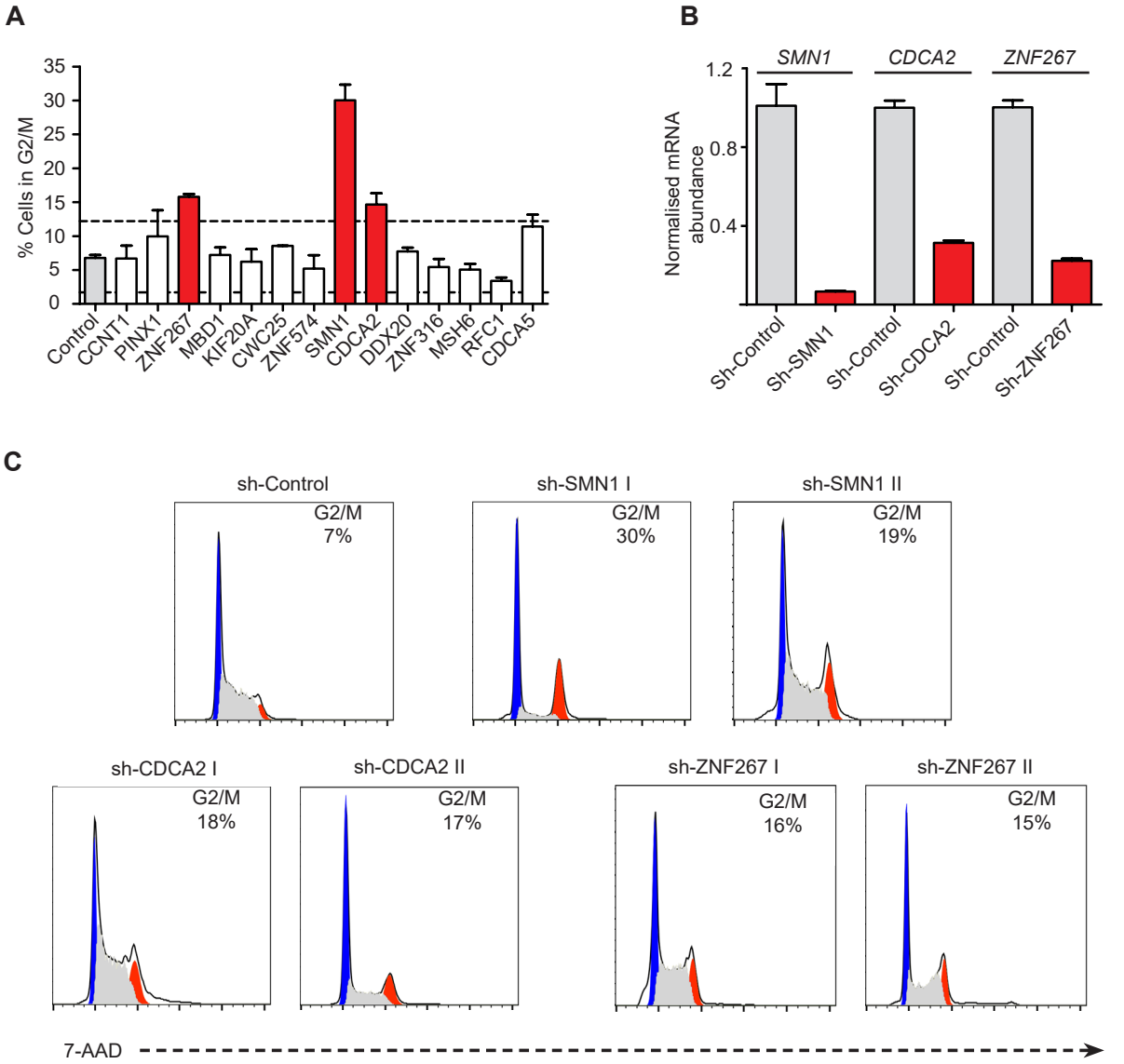
A
% Cells in G2/M
35
30
25
20
15
10
5
0
Control
CCNT1
PINX1
ZNF267
MBD1
KIF20A
CWC25
ZNF574
SMN1
CDCA2
DDX20
ZNF316
MSH6
RFC1
CDCA5
B
SMN1
CDCA2
ZNF267
Normalised mRNA abundance
1.2
0.8
0.4
Sh-Control
Sh-SMN1
Sh-Control
Sh-CDCA2
Sh-Control
Sh-ZNF267
C
sh-Control
G2/M
7%
sh-SMN1 I
G2/M
30%
sh-SMN1 II
G2/M
19%
sh-CDCA2 I
G2/M
18%
sh-CDCA2 II
G2/M
17%
sh-ZNF267 I
G2/M
16%
sh-ZNF267 II
G2/M
15%
7-AAD

Figure 7

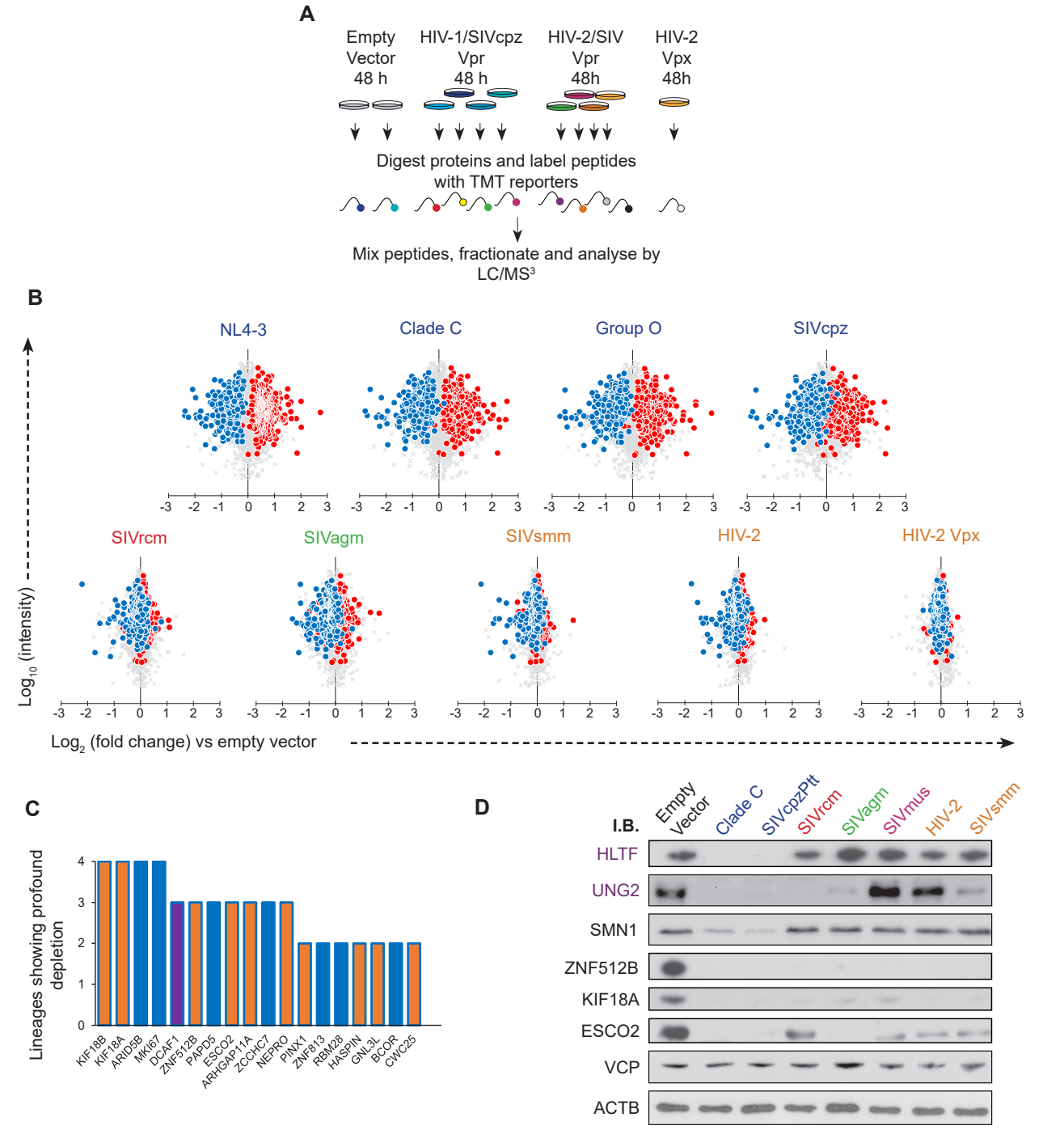
A
Empty Vector 48 h
HIV-1/SIVcpz Vpr 48 h
HIV-2/SIV Vpr 48h
HIV-2 Vpx 48h
Digest proteins and label peptides with TMT reporters
Mix peptides, fractionate and analyse by LC/MS3
B
NL4-3
Clade C
Group O
SIVcpz
SIVrcm
SIVagm
SIVsmm
HIV-2
HIV-2 Vpx
Log10 (intensity)
Log2 (fold change) vs empty vector
C
Lineages showing profound depletion
KIF18B
KIF18A
ARID5B
MKI67
DCAF1
ZNF512B
PAPD5
ESCO2
ARHGAP11A
ZCCHC7
NEPRO
PINX1
ZNF813
RBM28
HASPIN
GNL3L
BCOR
CWC25
D
I.B.
Empty Vector
Clade C
SIVcpzPtt
SIVrcm
SIVagm
SIVmus
HIV-2
SIVsmm
HLTF
UNG2
SMN1
ZNF512B
KIF18A
ESCO2
VCP
ACTB

Figure 7 - Supplement 1

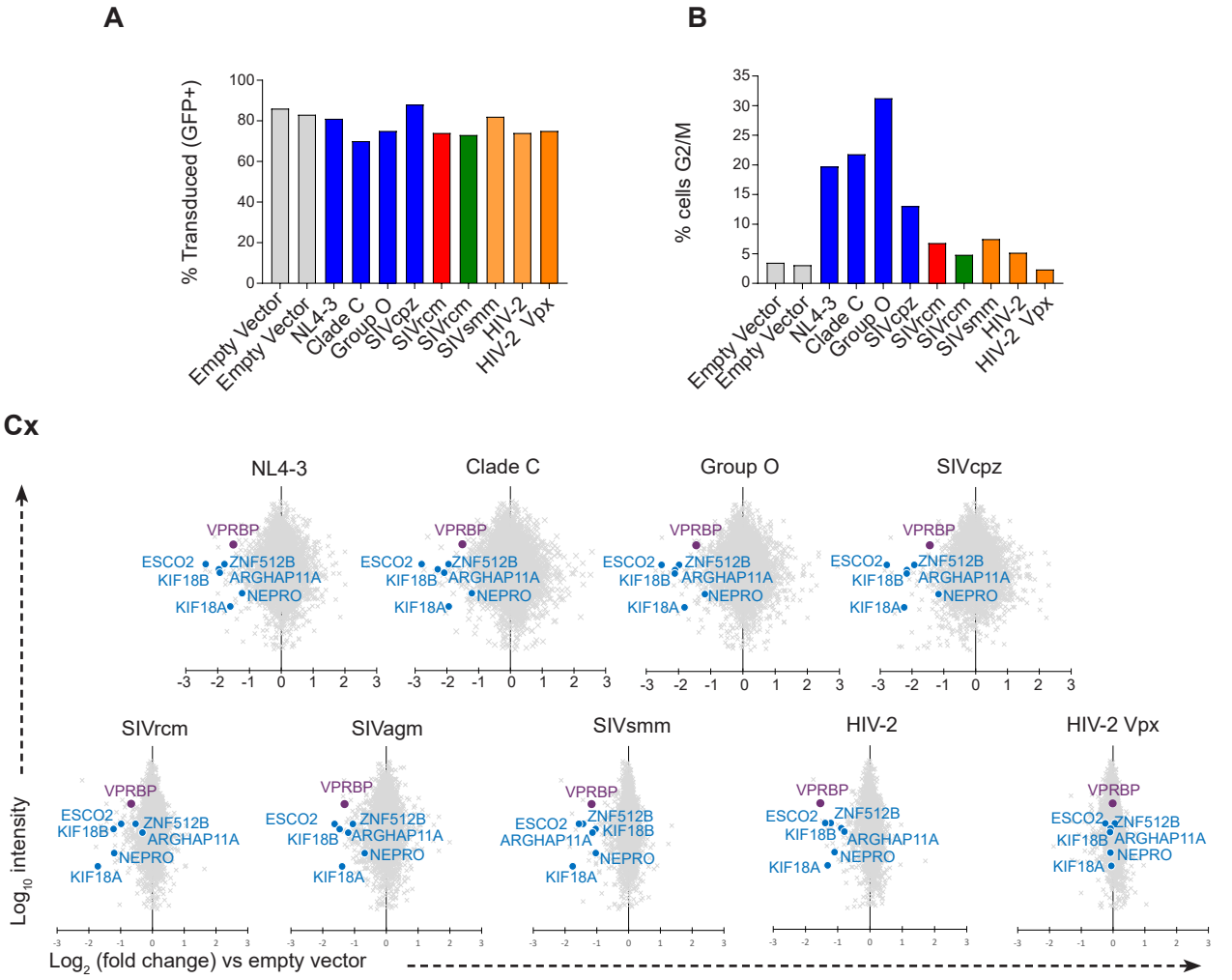

Figure 8

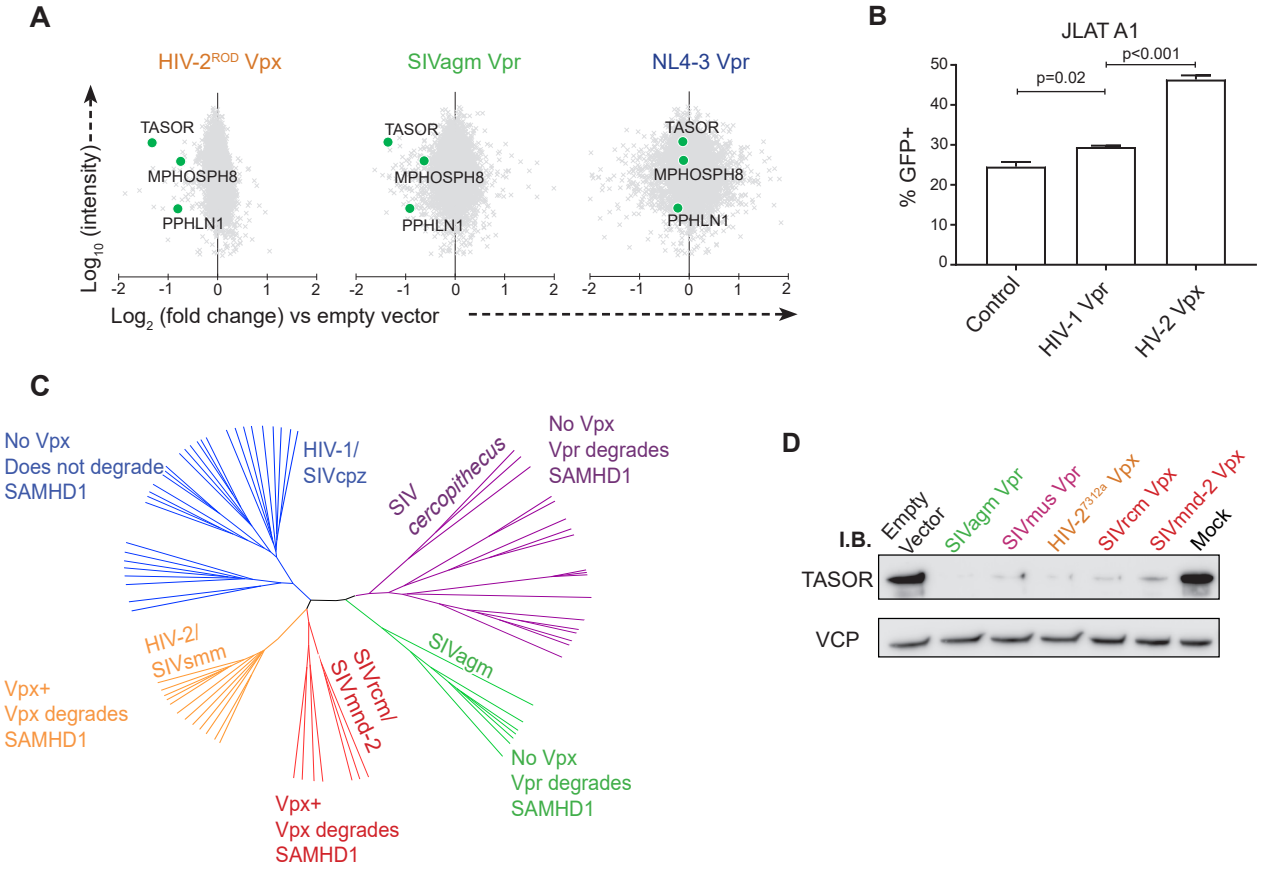
A
HIV-2ROD Vpx
SIVagm Vpr
NL4-3 Vpr
TASOR
MPHOSPH8
PPHLN1
Log10 (intensity)
Log2 (fold change) vs empty vector
B
JLAT A1
p=0.02
p<0.001
% GFP+
Control
HIV-1 Vpr
HIV-2 Vpx
C
No Vpx
Does not degrade
SAMHD1
HIV-1/
SIVcpz
SIV
cercopithecus
No Vpx
Vpr degrades
SAMHD1
HIV-2/
SIVsmm
Vpx+
Vpx degrades
SAMHD1
SIVrcm/
SIVmnd-2
SIVagm
No Vpx
Vpr degrades
SAMHD1
Vpx+
Vpx degrades
SAMHD1
D
I.B.
Empty Vector
SIVagm Vpr
SIVmus Vpr
HIV-2 Vpx
SIVrcm Vpx
SIVmnd-2 Vpx
Mock
TASOR
VCP

Figure 9

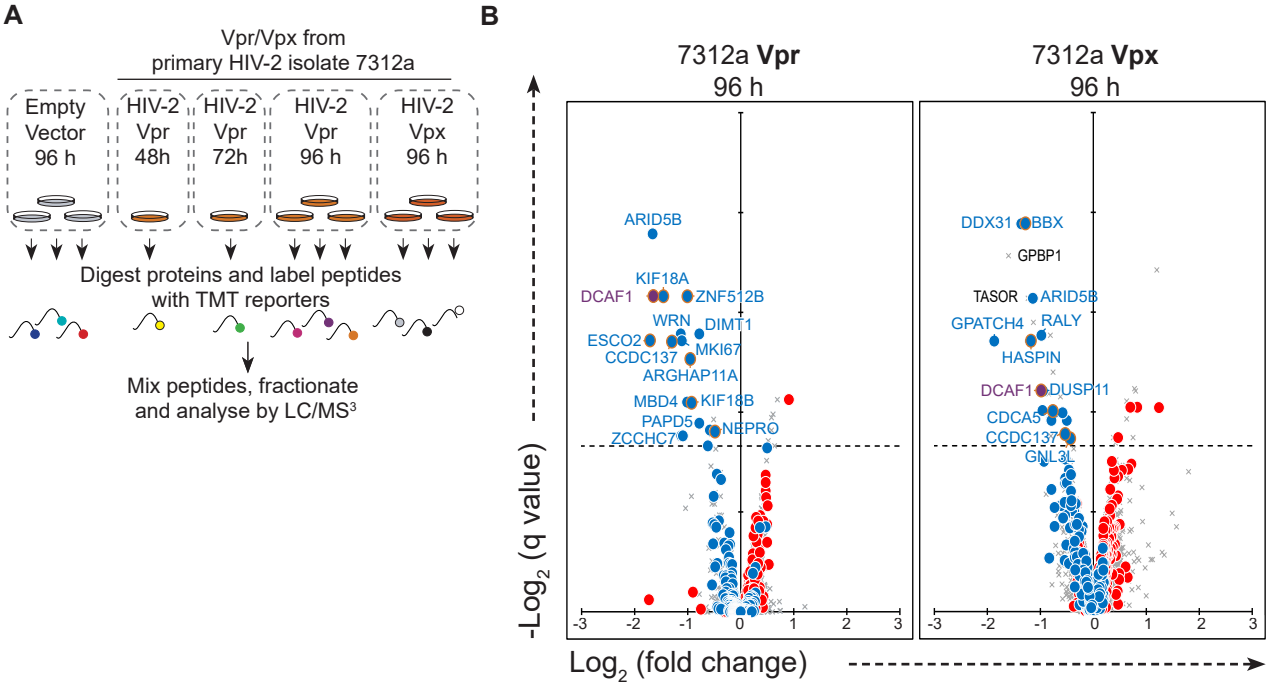
A
Vpr/Vpx from
primary HIV-2 isolate 7312a
Empty Vector 96 h
HIV-2 Vpr 48h
HIV-2 Vpr 72h
HIV-2 Vpr 96 h
HIV-2 Vpx 96 h
Digest proteins and label peptides with TMT reporters
Mix peptides, fractionate and analyse by LC/MS³
B
7312a Vpr 96 h
7312a Vpx 96 h
ARID5B
KIF18A
DCAF1
ZNF512B
WRN
DIMT1
ESCO2
MKI67
CCDC137
ARGHAP11A
MBD4
KIF18B
PAPD5
NEPRO
ZCCHC7
DDX31
BBX
GPBP1
TASOR
ARID5B
GPATCH4
RALY
HASPIN
DCAF1
DUSP11
CDCA5
CCDC137
GNL3L
-Log2 (q value)
Log2 (fold change)
-3
-2
-1
0
1
2
3

Table 2

Vpr **Species**	**Genbank Accession**	**Data presented in:**
HIV-1 $_{NL4-3}$	AF324493.2[78]	Figures 1-9.
HIV-1 $_{98BR004}$ (Clade C)	AAK31002.1[79]	Proteomics experiment & IB (Figure 9A-D)
HIV-1 $_{BCF09}$ (Group O)	CAA75954.1	Proteomics experiment (Figure 9A-C)
SIVcpzPtt $_{MB897}$	ABU53019.1[80]	Proteomics experiment & IB (Figure 9A-D)
SIVrcm $_{02CM8081}$	ADK78264.1[81]	Proteomics experiment & IB (Figure 9A-D)
SIVagm $_{Sab92018}$	ADO34202.1[82]	Proteomics experiment & IB (Figure 9A-D), I.B, (Figure 10D)
SIVsmm $_{E660}$	ANT86736.1[83]	Proteomics experiment & IB (Figure 9A-D)
HIV-2 $_{ROD}$	CAA28911.1[84]	Proteomics experiment (Figure 9A-C)
HIV-2 $_{7312a}$	AAL31354.1	I.B. (Figure 9D), Proteomics experiment, (Figure 11A-C)
SIVmus $_{01CM1239}$	ABO61047.1[85]	I.B. (Figure 9D), I.B. (Figure 10D)

Vpx

Species	**Genbank Accession**	**Data presented in:**
HIV-2 $_{ROD}$	AAB00766.1[84]	Proteomics experiment (Figure 9A-C)
HIV-2 $_{7312a}$	AAL31353.1	I.B. (Fig.9D), I.B. (Fig. 10D), Proteomics experiment, (Figure 11A-C)
SIVrcm $_{Ng411}$	AAK69676.1[86]	I.B. (Fig. 10D)
SIVmnd-2 $_{5440}$	AAO22477.1 [87]	I.B. (Fig. 10D)